Assessing shoreline orientation variation across diverse coastal environments

Abdulsalam, Mayowa Basit; Jaramillo, Camilo; de Freitas, Lucas; González, Mauricio; Antolínez, José A.Á.

DOI
10.1016/j.coastaleng.2025.104770

Publication date
2025

Document Version
Final published version

Published in
Coastal Engineering

Citation (APA)
Abdulsalam, M. B., Jaramillo, C., de Freitas, L., González, M., & Antolínez, J. A. Á. (2025). Assessing shoreline orientation variation across diverse coastal environments. *Coastal Engineering*, *200*, Article 104770. https://doi.org/10.1016/j.coastaleng.2025.104770

Coastal Engineering 200 (2025) 104770

Contents lists available at ScienceDirect

Coastal Engineering

journal homepage: www.elsevier.com/locate/coastaleng

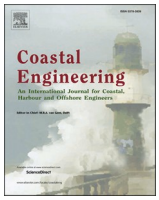

Assessing shoreline orientation variation across diverse coastal environments

Mayowa Basit Abdulsalam [a,*], Camilo Jaramillo [a], Lucas de Freitas [a], Mauricio González [a], José A.Á. Antolínez [b]

[a] Environmental Hydraulics Institute, Universidad de Cantabria, Avda. Isabel Torres, 15, Parque Científico y Tecnológico de Cantabria, 39011, Santander, Spain
[b] Department of Hydraulic Engineering, Faculty of Civil Engineering and Geosciences, Delft University of Technology, Delft, Netherlands

ARTICLE INFO

Keywords:
Coastal morphodynamics
Equilibrium-based shoreline evolution model
Shoreline rotation
Shoreline variability
Wave-driven sediment transport

ABSTRACT

Understanding and predicting shoreline variability at various temporal and spatial scales is vital for effective, data-driven coastal management. Shoreline position, a reliable indicator of beach morphological changes, has been assessed using complex numerical models. Recently, equilibrium-based shoreline evolution models (EBSEMs) have gained traction for their efficiency in simulating shoreline orientation, including cross-shore and rotational (longshore) changes. However, existing EBSEMs for shoreline rotation have been applied predominantly to microtidal beaches, with limited validation across diverse coastal environments.

This study evaluates the performance and scalability of the EBSEM proposed by Jaramillo et al. (2021) in modelling shoreline rotational variability at seven embayed beaches: Narrabeen Beach (Australia), Tairua Beach (New Zealand), Blackpool Beach (United Kingdom), Poniente Beach, Llevant Beach, Cala Millor Beach, and Moncofa Beach (Spain). These sites represent diverse environmental conditions in terms of sediment size, tidal regimes, monitoring frequency, and data types. The model was tested across full monitoring periods, elevation contours, and temporal resolutions.

Results show that EBSEM performs well across contrasting beach types, effectively capturing short-term and seasonal shoreline rotation patterns. However, reduced accuracy was observed in environments with high-energy events or human interventions, such as Poniente, Llevant, and Cala Millor beaches. Sensitivity analyses highlight the importance of temporal resolution and intertidal elevation in model performance.

While the EBSEM shows significant potential for broader application, further refinement is needed to better capture storm-driven and anthropogenic variability. These improvements would enhance its utility for coastal adaptation planning, hazard mitigation, and long-term shoreline management in the face of climate change.

1. Introduction

Shoreline variability refers to the changes in the position and shape of shorelines, which can occur over various temporal scales, ranging from daily to seasonal, and across different spatial scales, from hundreds of meters to kilometres (Bryan et al., 2013; Harley et al., 2011a). These variations can be attributed to a variety of environmental factors, including natural processes such as wave action, tides, sediment transport, and erosion, along with anthropogenic influences such as coastal development, land reclamation, and human intervention in coastal management (Harley et al., 2011a; Jaramillo et al., 2020; Miller and Dean, 2004).

Consequently, understanding and accurately predicting this variability has become increasingly important as it frequently involves nonlinear coastal processes. The significance of this understanding is emphasised by the fact that approximately 40 % of the world's population lives within 200 km of the coastlines (Creel, 2003). This value is expected to increase in the future due to coastal zone development, thereby resulting in increased pressure along the coastline and thus changing the natural processes of beaches around the world (Neumann et al., 2015). Additionally, coastal infrastructure is at risk due to significant shoreline movement. These shifts can make existing structures vulnerable, prompting the need for mitigation measures.

The complexity of coastal processes occurring at a beach is

* Corresponding author.
E-mail addresses: mayowa-basit.abdulsalam@alumnos.unican.es (M.B. Abdulsalam), jaramilloc@unican.es (C. Jaramillo), freitasl@unican.es (L. de Freitas), mauricio.gonzalez@unican.es (M. González), J.A.A.Antolinez@tudelft.nl (J.A.Á. Antolínez).

https://doi.org/10.1016/j.coastaleng.2025.104770
Received 26 December 2024; Received in revised form 24 March 2025; Accepted 29 April 2025
Available online 30 April 2025

inherently three-dimensional due to the dynamic interactions between hydrodynamic processes, such as wave and tide movements and sedimentary processes, including erosion, transport, and deposition (González et al., 2010). Factors like coastline shape, sediment characteristics, and environmental conditions such as wind and weather influence these interactions. As waves approach the shore, they interact with the underwater topography, causing variations in wave height and energy that affect sediment movement (Zhang et al., 2020). Additionally, the relationship between incoming waves and returning currents continually alters the landscape, emphasising the need to study these processes to understand coastal dynamics and the impacts of human activities and climate change.

However, in engineering applications, the current limitations of tools, formulations, and our understanding of these processes hinder a comprehensive three-dimensional analysis (González et al., 2010). To address this issue, an orthogonality hypothesis is proposed. This hypothesis posits that any beach movement can be effectively analysed by independently examining the longitudinal (longshore) and transversal (cross-shore) movements (de Vriend et al., 1993; González et al., 2010).

Since shoreline variability has been regarded as a reliable indicator that can be used to describe the overall changes in beaches at various spatiotemporal scales (Smith and Bryan, 2007), the morphodynamic processes that influence the shoreline position will be possible to simulate through the integration of the longshore, cross-shore and gradient or curvature processes. Research has shown that cross-shore processes such as overwash due to storm and wave-driven beach profile dynamics are responsible for short-term variability. At the same time, alongshore gradients in longshore sediment transport have been identified as the drivers for long-term variability of the shoreline (Harley et al., 2011b).

To evaluate the variability in an embayed beach, shoreline changes can be simplified into three movements (Ratliff and Murray, 2014): cross-shore migration (Fig. 1a), representing sediment movement perpendicular to the shoreline (Davidson et al., 2013; Palalane et al., 2016; Robinet et al., 2018; Yates et al., 2009): beach breathing (Fig. 1b), denoting changes in shoreline curvature (Ratliff and Murray, 2014); and beach rotation (Fig. 1c–d), the primary focus of this study, involving the landward or seaward movement of one end of a beach with a corresponding reverse pattern at the other end (Klein et al., 2002; Thomas et al., 2010; Turki et al., 2013a).

To properly assess and quantify shoreline evolution, the scientific community has attempted to develop methods to predict shoreline variability on medium to long-term scales. The existing shoreline evolution models, 3D topo-bathymetric models (e.g. de Vriend et al., 1993), multi-line shoreline models (e.g. Hanson and Larson, 1990), one-line shoreline models (e.g. Hanson and Kraus, 1991; Pelnard-Considère, 1957), combined models (e.g. Antolínez et al., 2019; Robinet et al., 2018; Vitousek et al., 2017), and equilibrium-based shoreline evolution models (e.g. Blossier et al., 2017; Jaramillo et al., 2021; Miller and Dean, 2004; Turki et al., 2013a; Yates et al., 2009) have been mostly considered.

All these models require long data series and contain parameterisations of physical processes with accompanying calibration, making them computationally intensive except for the equilibrium-based shoreline evolution models (EBSEMs), which are the simplest, computationally efficient, and can be used for forecasting the daily to long-term morphological changes in various coastal settings (Davidson and Turner, 2009). Due to EBSEM's reduced complexity, ease of use, and effectiveness, which are well described in the methodology section, its use has increased in recent years. It has been designed to replicate the shoreline variability based on the type of movement. Some focus on cross-shore transport, exemplified by the models proposed by Miller and Dean (2004) and Yates et al. (2009), among others. On the other hand, models tailored for longshore sediment transport are responsible for shoreline rotation, such as those by Jaramillo et al. (2021) and Turki et al. (2013a).

While extensive research has focused on cross-shore shoreline dynamics, rotational shoreline movement remains comparatively underexplored despite its significance in coastal engineering. Also, the existing shoreline rotation models have been applied to only a handful of case studies, raising concerns about their applicability across diverse coastal environments. This study addresses these limitations by advancing the scalability and predictive accuracy of EBSEMs for broader coastal applications through the following objectives: (1) assessing the capability of EBSEM to predict shoreline rotation across diverse coastal environments, each with its varying hydrodynamic and morphological characteristics; (2) identifying the uncertainties that affect EBSEM performance, including natural variability of coastal environments and model-related uncertainties; and (3) proposing methodological approaches to improve the model robustness and global applicability for coastal engineering applications.

To support these objectives, this study introduces methodological advancement that could enhance the scalability and robustness of EBSEM. Specifically, the model sensitivity is evaluated across different

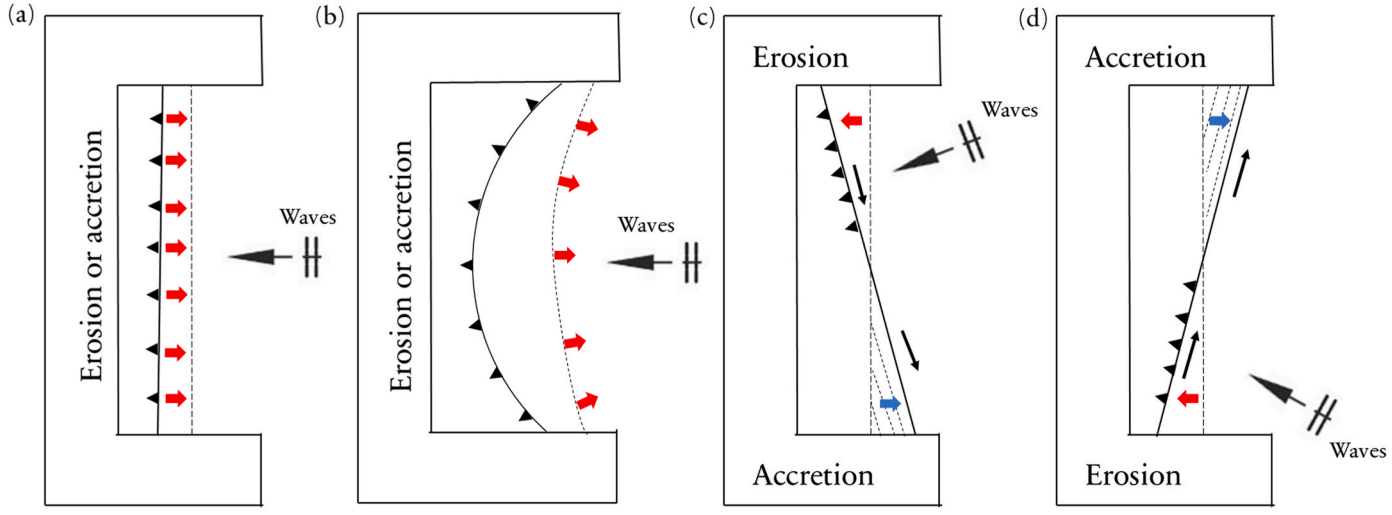

Fig. 1. Shoreline variability movement. (a) Cross-shore movement with incoming waves perpendicular to the shoreline causing sediment transport perpendicular to the coastline, (b) Beach breathing with incoming waves perpendicular to the shoreline causing changes in the shoreline curvature, (c–d) Rotation movement, where: (c) Simplified model of beach rotation with oblique wave arriving on an embayed beach causing alongshore sediment transport downdrift leading to accretion and erosion updrift, and (d) A reversing oblique wave direction subsequently creates accretion updrift and erosion downdrift.

temporal resolutions, ranging from daily to monthly shoreline observations, and across multiple shoreline elevation contours within the intertidal zone. These analyses enhance our understanding of how data resolution and vertical shoreline variability influence the model performance.

By addressing these challenges, this study aims to advance shoreline rotation modelling by providing valuable insights for evidence-based coastal management practices. Improving the predictive capability of EBSEMs will enable more reliable shoreline evolution predictions, which is essential for effective coastal management amid climate change and human interventions. These advancements will strengthen resilient defence strategies and support sustainable adaptation measures, ensuring long-term coastal protection (Azorakos et al., 2024; D'Anna et al., 2024).

The remainder of this paper is organised as follows. First, the study sites are presented in Section 2. The wave climate and shoreline orientation data are presented in Section 3. The overall methodology used for this study is described in Section 4, starting with the model description with underlying assumptions and hypotheses, calibration method and performance evaluation. The model results are shown in Section 5. A discussion of the model's performance, sensitivity and limitations is presented in Section 6. Finally, the main conclusions are summarised in Section 7.

2. Study sites

This study assesses the predictive capability of EBSEM in simulating shoreline rotation across seven distinct coastal environments with multi-annual shoreline monitoring programs. The selected study sites, Narrabeen Beach, Tairua Beach, Poniente Beach, Llevant Beach, Cala Millor Beach, Moncofa Beach, and Blackpool Beach, were chosen to represent a diverse range of hydrodynamic conditions, sediment compositions, and anthropogenic influences. These sites represent diverse wave climates and tidal regimes, ranging from microtidal to macrotidal, and exhibit sediment characteristics varying from sand to gravel. Additionally, the study sites incorporate multiple shoreline monitoring approaches, utilising various data sources such as field surveys, video monitoring, and satellite imagery. The selected beach lengths range from a few hundred meters to several kilometers, allowing for an assessment of shoreline evolution processes across different spatial scales. By integrating these diverse datasets, the study evaluates how shoreline rotation processes vary across different coastal settings.

Hence, this section provides an overview of the selected study sites (Table 1 and Fig. 2), detailing their wave characteristics, which are the main driving force of the selected EBSEM, and the derived shoreline orientation datasets used in the analysis.

2.1. Collaroy-Narrabeen Beach, Australia

Collaroy-Narrabeen Beach is located approximately 20 km north of Sydney Harbour along the coastline of the Sydney metropolitan area (Fig. 2a). This 3.6 km embayed beach system is bordered by Narrabeen Headland in the north and Long Reef Point, a 1.5 km-long headland, in the south. The site comprises two beaches: Narrabeen Beach to the north and Collaroy Beach to the south. A small, intermittently open lagoon exists at the northern end (Morris and Turner, 2010). Sediments are predominantly homogeneous fine-to-medium quartz sand with a median grain size (D_{50}) of ≈0.3 mm and a carbonate content of ~30 %. Minimal sediment interaction occurs between the embayment, the lagoon, and adjacent beaches, effectively closing the system (Harley et al., 2011a). The beach is classified as wave-dominated (Short, 2006), exhibiting an intermediate morphodynamic state with seasonal transitions towards reflective or dissipative conditions (Wright et al., 1985).

2.2. Tairua Beach, New Zealand

Tairua Beach is a 1.2 km-long microtidal sandy beach located on the Coromandel Peninsula, North Island in New Zealand (Fig. 2b). It is flanked by Pumpkin Hill to the north and Paku Hill to the south, with the latter extending approximately 600 m seaward from the dune foot. Offshore, Shoe Island, situated 3 km east of Paku Hill and spanning over 1 km from south to north, partially shelters the beach from incoming waves. The rocky coasts along its eastern coastline are interrupted by many embayed beaches caused by local sediment supply by rivers or bypassing effects (Hart and Bryan, 2008). The beach is primarily exposed to long-traveling easterly and north-easterly swells and storm waves from the Pacific Ocean, with an average wave direction of 53° toward the north (Jaramillo et al., 2021). The beach sediments consist of quartz-rich sand with a median grain size (D_{50}) ranging between 0.30 and 0.60 mm (Blossier et al., 2017; Smith and Bryan, 2007). The tidal range varies from 1.2 m during neap tide to 2.0 m during spring tide (Black et al., 2016).

2.3. Poniente and Llevant Beach, Spain

Poniente and Llevant Beaches are the two main beaches of Benidorm, located on the Spanish Mediterranean coastline. Poniente Beach is 3 008 m long, while Llevant Beach, also known as Levante Beach, extends 2 261 m (Fig. 2c). Both beaches are classified as microtidal, with a maximum tidal range of ~0.3 m and a mean sediment grain size (D_{50}) of ≈0.30 mm (Aragonés et al., 2015; Ecolevante, 2006). Both beach systems are closed embayments formed by natural headlands, exhibiting minimal sediment exchange with adjacent systems.

2.4. Cala Millor beach, Spain

Cala Millor Beach is a semi-embayed microtidal sandy beach, 1.7 km long and 35 m wide, situated on the northeastern coast of Mallorca in the western Mediterranean Sea (Fig. 2d). The beach is bounded by "Cape des Pinar" to the north and "Punta de n'Amer" to the south, with steep submarine slopes beneath these cliffs. *Posidonia Oceanica* meadows at the central part of the bay make the bathymetry there different as they follow the same regular and shallow slope topography of the *Posidonia Oceanica.* Also, they act as a cover for sediment exchange and attenuation to the incoming wave (Abreu et al., 2020). The beach is composed of well-sorted medium-to-coarse biogenic carbonate sands with a median grain size (D_{50}) of 0.33 mm varying over the cross-shore distance by ± 0.3 mm, depending on depth (Gómez-Pujol et al., 2011).

Table 1
Summary of study sites and survey data.

Site	D_{50} (mm)	Average Length (m)	Tidal Range	Shoreline Orientation Data	Frequency of Monitoring	Monitoring Period
Narrabeen Beach, Australia	0.30	3 600	Microtidal	Field surveys	Monthly	1976–2019
Tairua Beach, New Zealand	0.45	1 200	Microtidal	Video camera	Daily	1999–2013
Poniente Beach, Spain	0.30	3 008	Microtidal	Satellite Images	Monthly	1984–2022
Llevant Beach, Spain	0.30	2 261	Microtidal	Satellite Images	Monthly	1984–2022
Cala Millor Beach, Spain	0.33	1700	Microtidal	Video camera	Biweekly	2011–2020
Moncofa Beach, Spain	>4.00	330	Microtidal	Satellite Images	Monthly	2017–2020
Blackpool Beach, United Kingdom	5.00	650	Macrotidal	Field Surveys	Six-Monthly	2007–2020

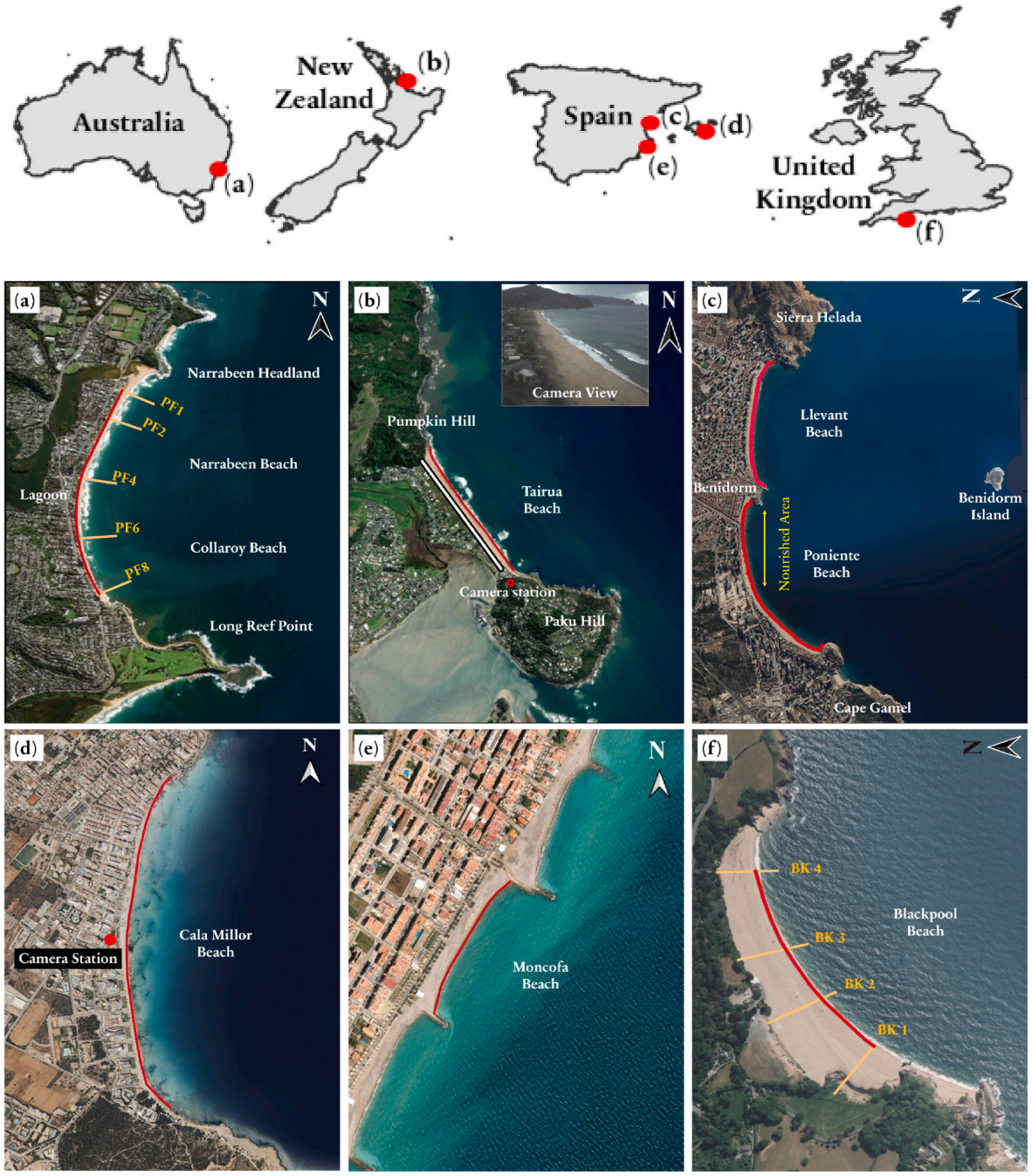

Fig. 2. Location of study sites: (a) Narrabeen-Collaroy Beach, Australia, highlighting the location of the five monthly survey transects (PF1, PF2, PF4, PF6, PF8); (b) Tairua Beach, New Zealand, including a reference line to estimate the shoreline position and the camera station with a corresponding view; (c) Poniente Beach and Llevant Beach, Spain, including the nourished area on Poniente Beach in 1991; (d) Cala Millor Beach, Spain, including the camera station; (e) Moncofa Beach, Spain; and (f) Blackpool Beach, United Kingdom, highlighting the location of the four survey transects (BK1, BK2, BK3, BK4).

2.5. *Moncofa Beach, Spain*

Moncofa Beach is an urbanised microtidal coastline between the ports of Castellón and Sagunto along the Spanish Mediterranean coast (Fig. 2e). The beach system consists of artificial embayed beaches separated by groins. The sediment sizes range from fine sands to pebbles, reflecting variability within the constructed system (Gomes da Silva et al., 2024; Rodríguez-Santalla et al., 2021).

2.6. *Blackpool Beach, United Kingdom*

Blackpool Beach, also known as Blackpool Sands, is one of four interconnected gravel barrier beaches in Start Bay, located along the south coast of Devon, Southwest England (Fig. 2f). It is a 650 m-long macro-tidal beach with tidal ranges of approximately 2 m during neap tides and up to 5 m during spring tides (Chadwick et al., 2005; McCarroll et al., 2023). The beach face is steep and reflective ($\tan\beta = 0.1$), with a median grain size (D_{50}) ranging between 2 and 10 mm (Wiggins et al., 2019)

3. Data

This section presents the wave condition of the studied sites and the corresponding derived shoreline position datasets.

3.1. Wave climate data

This subsection presents the wave characterisation of datasets of the studied area as the main driving force of the JA21 model.

3.1.1. Narrabeen Beach

The wave climate for Narrabeen Beach was derived from the IHCantabria Global Ocean Waves (GOW) reanalysis database based on a 0.5° global mesh (Perez et al., 2017). This dataset, calibrated and validated using buoy and satellite altimetry data (Reguero et al., 2012), provides hourly sea state parameters such as significant wave height (Hs), peak period (Tp), and wave direction. For Narrabeen Beach, data from an offshore point at −34.0° latitude and 151.5° longitude, with a depth of approximately 218 m, spanning 1979–2019, was utilised. Statistical analysis using wave roses (Fig. 3) shows that Hs ranges from 0.4 to 9.0 m. Waves predominantly originate from the South-Southeast 20 % of the time, with the most energetic waves from the South and Southeast occurring around 17 % and 14 % of the time, respectively. Seasonal patterns indicate that east-northeast waves dominate in summer, while waves are primarily from the south during winter.

3.1.2. Tairua Beach

The wave data for Tairua Beach used for this research were sourced from the University of Auckland's Shoreshop hindcast dataset (1979–2016) at −36.988° latitude and 175.864° longitude, 600 m offshore at an 8 m depth (Montaño et al., 2019). Analysis indicates (Fig. 3) that the most frequent waves come from the northeast and east-northeast 48 % of the time, with Hs ranging from 0.1 to 4.4 m with an average of 1.4 m and peaking at 6 m during storms (Smith and Bryan, 2007). Seasonal variations show a dominance of east-northeast waves in austral winter (June–August) and northeast waves in summer (December–February).

3.1.3. Poniente and Llevant Beach

Wave climate for Poniente and Llevant Beaches was derived from the GOW database for an offshore point at 38.417° latitude and −0.167° longitude at an 82 m depth, covering 1979–2022. Wave roses reveal (Fig. 3) that considering all months, the most frequent waves originate from the East-Southeast (24 %), Southeast (21 %) and South (15 %), with Hs ranging from 0.1 to 4.0 m. This is due to these beaches not only facing the south but also being conditioned by Benidorm Island (which reduces the incoming wave on Llevant Beach by 10 %), Cape Gamell to the west, and the massif of Sierra Helada to the east (reduces incoming wave by almost 50 % on Llevant Beach compared to Poniente), which protect these beaches from the incoming wave from the east, thereby reducing the impact of storms compared to other parts of the Spanish Mediterranean coast (Fig. 3) (Amores et al., 2020; Aragonés et al., 2015; Toledo et al., 2022). During summer, most waves also come from the East-Southeast; in winter, the waves come from the South, South-Southeast, East, and East-Northeast.

3.1.4. Cala Millor beach

Wave data for Cala Millor Beach were obtained from the GOW database at 39.5834° latitude and 3.5° longitude, with a depth of 56 m (1979–2017). The statistical analysis reveals (Fig. 3) that the most frequent waves are from the North-Northeast (27 %) and South-Southeast (12 %), reflecting the beach's semi-enclosed, east-facing configuration. The Hs and Tp ranges from 0.03 to 6.0 m and 4.0–10.0 s, with an average of 8.7 s (Enríquez et al., 2017; Fernández-Mora et al., 2023; Tintoré et al., 2009).

3.1.5. Moncofa Beach

Wave climate data for Moncofa Beach, spanning 1979–2020, were obtained from an offshore GOW point at 39.7° latitude and −0.0833° longitude at 30 m depth. Wave roses (Fig. 3) reveal dominant storm events originating from the East-Northeast around 25 % of the time, with the most frequent swell from the east around 20 % of the time. For the summer months, the frequent waves come from the Southeast around 33 % of the time, while during winter, most waves come from the East-Northeast, thereby depicting a strong seasonal pattern. The coastal configuration and the bimodal wave climate in the area cause a seasonal shoreline rotation, a process reported previously on other beaches of the Spanish Mediterranean coast (Castelle et al., 2020; Ojeda and Guillén, 2008). The Hs and Tp range from 0.03 to 4.0 m and 0.5–11.5 s, respectively.

3.1.6. Blackpool Beach

Blackpool Beach data were sourced from the GOW database at 50.25° latitude and −3.50° longitude, with a 47.5 m depth covering 1979–2022. Analysis (Fig. 3) shows that the most frequent and energetic waves come from the West-Southwest at around 47 % of the time during all months and 60 % of the time during summer. In contrast, during winter, the most frequent waves come from the West-Southwest 45 % of the time, and the most energetic, which comes from the Southwest, is around 27 % of the time.

3.2. Shoreline orientation data

This subsection presents the shoreline position datasets used in this study. This dataset was acquired from multiple sources which includes satellite imagery, video monitoring, and field measurements, to analyse the shoreline orientation.

3.2.1. Narrabeen Beach

Shoreline orientation data at Narrabeen Beach (Table 1) were obtained from monthly field surveys conducted between 1976 and 2019 as part of the Narrabeen-Collaroy monitoring program (Harley et al., 2011a). This dataset includes beach profile measurements at five cross-shore locations (PF1, PF2, PF4, PF6, and PF8; Fig. 2a). During the first three decades, simple and traditional survey techniques were employed, transitioning to advanced methods such as RTK-GPS from 2004 onwards (Turner et al., 2016). Each profile was surveyed at 10 m cross-shore intervals during low tide from a fixed benchmark at the landward limit.

For each field campaign, measurements of the five beach profiles were used to define the complete coastline. Fig. 4 shows the beach orientation index (BOI) (Eq. 1), which is a metric that indicates whether a beach's orientation is predominantly clockwise or anticlockwise compared to its long-term average (Harley et al., 2011b). By definition, a positive BOI represents a clockwise (CW) beach orientation with respect to the long-term average, while a negative BOI represents a counterclockwise (CCW) beach orientation. This index is essential to assess how a beach rotates with respect to coastal processes and climate change (Harley et al., 2015).

$$BOI(t) = 10\frac{(\alpha_s(t) - \overline{\alpha_s(t)})}{std(\alpha_s(t))} \quad (1)$$

Where $\alpha_s(t)$ is the shoreline orientation at time "t", $\overline{\alpha_s(t)}$ is the time-averaged of the shoreline orientation and $std(\alpha_s(t))$ is the standard deviation.

The evolution of the BOI over 43 years of analysis highlights multiple rotation events (Fig. 4a). Clockwise rotation events were prominent from 1992 to 1994, while counterclockwise rotations were dominant between 2007 and 2015. The peak clockwise rotation was recorded in October 2018, whereas the most pronounced counterclockwise rotation occurred in April 1981.

3.2.2. Tairua Beach

Shoreline orientation data for Tairua Beach (Table 1) were sourced from the Shoreshop monitoring system, based on daily video recordings collected over 15 years (1999–2013) by a camera installed on Paku Hill

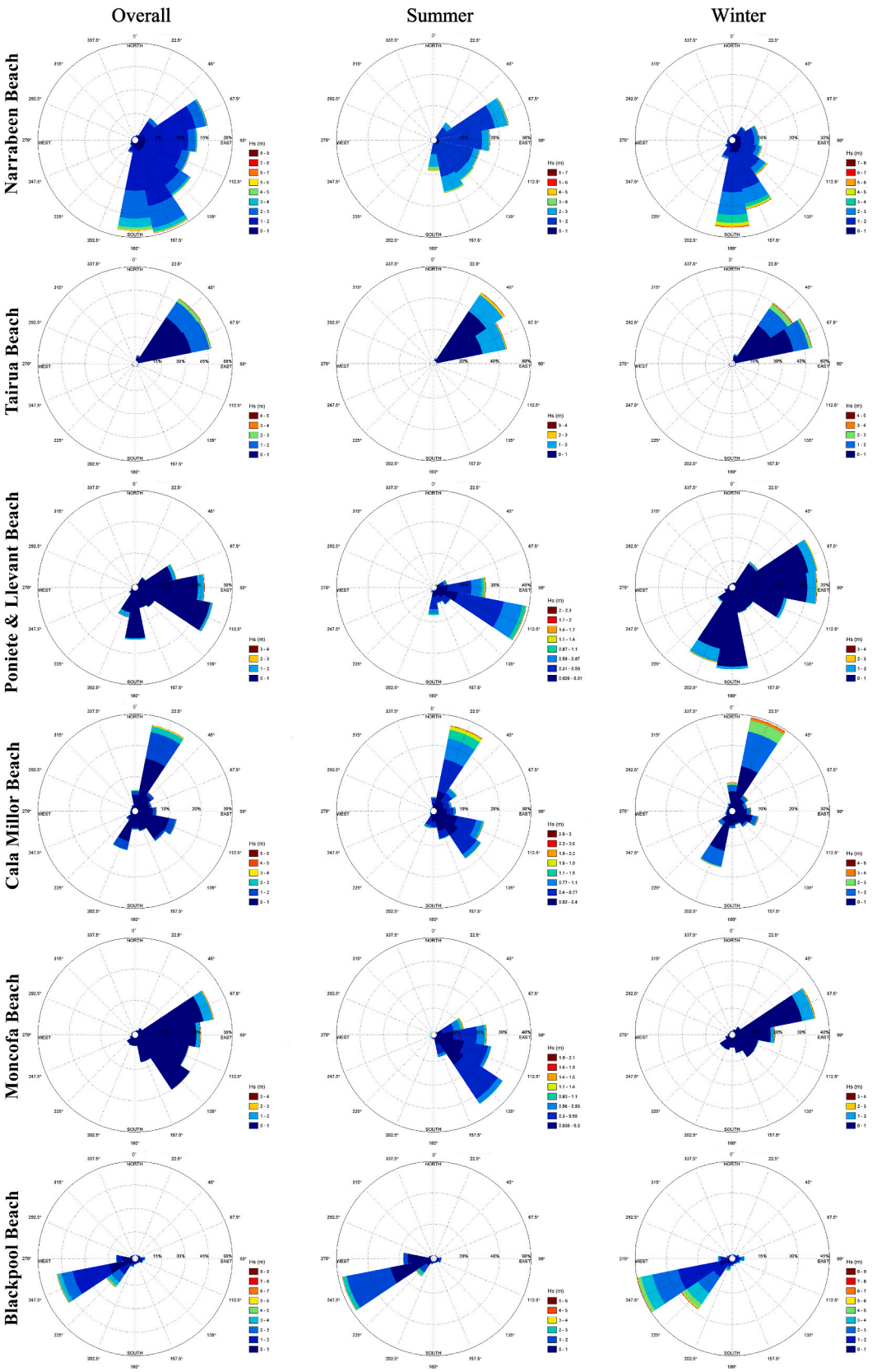

Fig. 3. Directional wave rose of Hs for study sites, categorised by all months, summer months and winter months. For study sites in the Southern Hemisphere (Narrabeen Beach and Tairua Beach), June, July, and August were considered winter months, while December, January and February were categorised as summer. In contrast, in Northern Hemisphere study sites (Poniente Beach, Llevant Beach, Cala Millor Beach, Moncofa Beach, and Blackpool Beach.), these periods were reserved, with December, January, and February considered for winter, and June, July and August classified as summer.

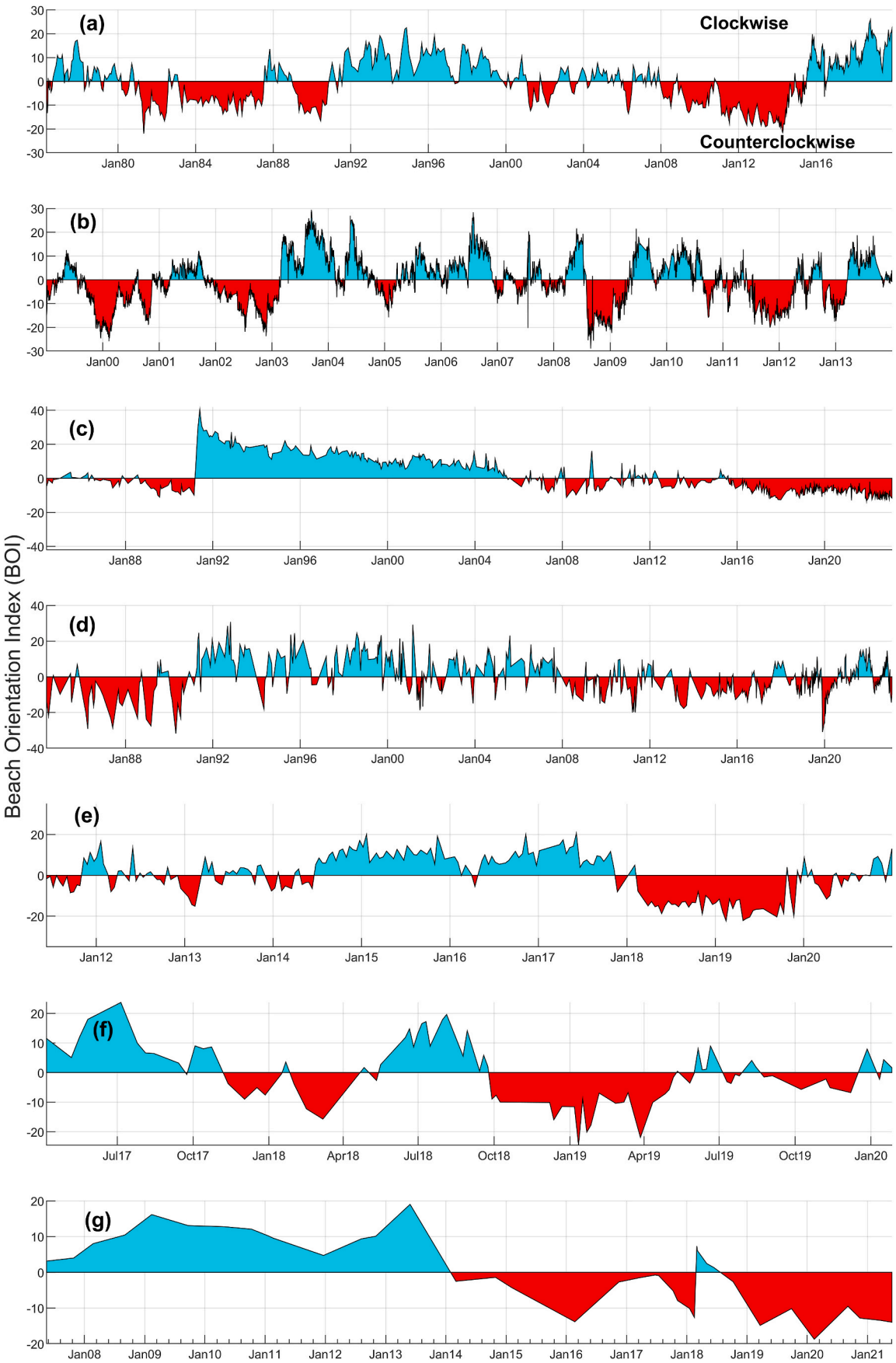

Fig. 4. Evolution of the beach orientation index (BOI) at (a) Narrabeen Beach, (b) Tairua Beach, (c) Poniente Beach, (d) Llevant Beach, (e) Cala Millor Beach, (f) Moncofa Beach, and (g) Blackpool Beach.

in the month of September 1997 at an elevation of 70 m (Almar et al., 2008; Montaño et al., 2019). Funded by the Waikato Regional Council and the National Institute of Water and Atmospheric Research (NIWA), this system captured the southern section of the beach (Fig. 2b). Processed by the University of Auckland, the video data provide a detailed time series of coastline variability (Table 1).

The 14-year BOI record for Tairua Beach reveals significant rotational behaviour (Fig. 4b). Clockwise rotation occurred between March 2005 and January 2007, with the most pronounced clockwise position in September 2003. In contrast, counterclockwise rotation was observed throughout 2002, peaking in August 2008.

3.2.3. Poniente and Llevant Beach

For Poniente and Llevant Beaches shoreline orientation data, this study employs a time series of the shoreline variability provided by the Geo-Environmental Cartography and Remote Sensing Group (CGAT) at the Polytechnic University of Valencia (UPV). This dataset consists of water lines extracted from Landsat and Sentinel satellite images, which were then processed to obtain shoreline positions from 1984 to 2022 (Table 1).

For Poniente Beach, the 38-year BOI data (Fig. 4c) indicate rotational trends corresponding to natural processes and anthropogenic interventions. The beach displayed its most counterclockwise orientation in December 2021. In May 1991, a significant clockwise rotation coincided with nourishment activities, involving 710,847 m^3 of sand deposition along a 1 305 m stretch, widening the beach by an average of 70 m (Aragonés et al., 2015; MOPT, 1991; Toledo et al., 2022). This nourishment was due to the coastal erosion the beach has suffered in previous years. Llevant Beach also experienced several rotational events (Fig. 4d), with the most clockwise orientation occurring in October 1992 and the most counterclockwise orientation in April 1990.

3.2.4. Cala Millor beach

Cala Millor's shoreline orientation data were obtained from the SOCIB Data Catalog processed by the Balearic Islands Coastal Observing and Forecasting System (Fernández-Mora et al., 2023). These publicly available datasets are from five video cameras located at 39.59° latitude and 3.38° longitude, at an elevation of approximately 46 m, recording images at 7.5 Hz during daylight hours (Fernández-Mora et al., 2023). These shoreline positions from June 2011 to December 2020 are then digitised biweekly from georeferenced plan view images (ETRS89), calibrated intrinsically and extrinsically (Table 1).

Over the ten years of BOI data, Cala Millor Beach exhibited distinct rotational dynamics (Fig. 4e). Clockwise rotation dominated from June 2014 to March 2016, peaking in June 2017. Conversely, counterclockwise rotation was recorded from January 2018 to December 2019, with the maximum counterclockwise position in February 2019.

3.2.5. Moncofa Beach

Shoreline orientation data for Moncofa Beach (Table 1) were sourced from the European Space Agency's EOEP-5 Coastal Erosion Project (Gomes da Silva et al., 2024). These data comprised waterlines derived from Landsat 5, Landsat 8, and Sentinel-2 images (April 2017–January 2020), corrected using tide gauge data from Puerto del Estado and local beach slope measurements.

The three-year BOI data for Moncofa Beach (Fig. 4f) illustrates rotational variability. A clockwise rotation was observed from May to October 2018, while a counterclockwise rotation prevailed from October 2018 to May 2019. The beach's most clockwise orientation was in July 2017, and the most counterclockwise position occurred in January 2019.

3.2.6. Blackpool Beach

Shoreline orientation data for Blackpool Beach from 2007 to 2021 (Table 1) were obtained from the South West Coastal Monitoring Program, operated by the Coastal Processes Research Group (CPRG) and the Plymouth Coastal Observatory (McCarroll et al., 2023). Surveys at four cross-shore transects (BK1–BK4; Fig. 2f) utilised RTK-GNSS during spring tides. These profiles are being surveyed semiannually to annually on foot using RTK-GNSS during spring tide extends from the onshore of the barrier crest down to the near spring low tide level, which is between −1 and −2 m Ordnance Datum Newlyn (ODN) (McCarroll et al., 2023).

The 14-year BOI record for Blackpool Beach shows clear rotational events (Fig. 4g). Clockwise rotation was prominent between 2013 and 2014, peaking in May 2013. Counterclockwise rotation was sustained from 2013 to December 2018, reaching its maximum extent in February 2020.

4. Methodology

This section provides a comprehensive explanation of the overall methodology used for this study, starting from the data processing, model description with underlying assumptions and hypotheses, and performance evaluation.

4.1. Model description

Among the limited number of EBSEMs for rotation movement in the literature, the model developed by Jaramillo et al. (2021), hereafter referred to as JA21, was used in this study to model the shoreline orientation evolution of diverse coastal environments, being the most recent model among others. This model is based on the following kinetic equation:

$$\frac{d\alpha_s(t)}{dt} = L^{\pm} P \Delta\alpha_s(\theta) \tag{2}$$

Where $\alpha_s(t)$ represent the shoreline orientation (°) at the time "t" and $L^{\pm}$ present the proportionality constants ($m^{-2}h^{-2}$); L^{+} is equivalent to clockwise shoreline rotation and L^{-} equivalent to the counterclockwise rotation. P (m^2s), the incident wave power can be defined as the model weighting factor resulting from the product of the squared of the significant wave height, Hs^2 (m^2), and the peak period, Tp (s).

$$P = Hs^2 \cdot Tp \tag{3}$$

$\alpha_s(\theta)$ (see Eq. 4) is the shoreline orientation disequilibrium.

$$\alpha_s(\theta) = \alpha_s - \alpha_{seq} \tag{4}$$

Where α_{seq} is the asymptotical equilibrium shoreline orientation, which is considered to be a linear relationship between the direction of the incident waves and the equilibrium shoreline orientation (see Eq. 5). It is crucial to emphasise that, in the case of evaluating a theoretical beach case, one could anticipate that $\alpha_{seq} \cong \theta$ the shoreline is perfectly straight, and the incident wave direction, θ, is uniform throughout the entire beach length. However, if one assumes that the wave conditions outside the active beach profile are the model forcing, there is a proportional relationship between α_{seq} and θ.

$$\alpha_{seq} = \frac{\theta - b}{a} \tag{5}$$

Where $a(-)$ and $b(^\circ)$ are empirical parameters corresponding to the y-intercept and slope coefficient, respectively, in a linear relationship between the equilibrium wave direction and the shoreline orientation.

The equilibrium shoreline orientation has been defined as the equilibrium wave direction function (EWDF) for a given wave direction. This function relates to the best adjustment between measurements, distinguishing positions that will rotate clockwise from ones that will rotate counterclockwise. Since the approach to equilibrium in this instance is exponential, the following is the form of the solution to equations (2)–(6):

$$\alpha_s(t) = \left(\alpha_s - \alpha_{seq}\right) e^{-L^{\pm} P t} + \alpha_{seq} \tag{6}$$

To summarise, the model formulation has four calibration parameters (a, b, L^+, and L^-). The coastline rotation rate (either clockwise or counterclockwise) is controlled by $L^{\pm}$, while parameters a and b establish the equilibrium condition (EWDF) and are calculated from the available surveys taken into consideration for calibration.

4.2. Model hypotheses and basic assumptions

The equilibrium shoreline evolution model selected for this study uses a series of assumptions and hypotheses. Beach rotation is assumed to be independent of other beach movements, i.e., not influenced by beach breathing or cross-shore migration. Hence, the beach rotation has been defined as dependent on the wave power and direction of incident waves. The model assumes a beach as a linear planform and a constant beach profile to separate shoreline movement. Based on the definition of beach rotation by Turki et al. (2013b, 2013a) as the lateral migration of sand towards opposite ends of an embayment, the model assumes that shoreline advancement and retreat are caused mainly by alongshore currents rather than wave height gradients, showing slight variation in wave height along the beach.

For the shoreline orientation, α_s, this model uses a procedure similar to that of Harley et al. (2014) and (Turki et al., 2013a). The procedure involves 1) the removal of time-averaged dry beach width from all recorded data, 2) fitting these demeaned data using linear regression, and 3) determining the shoreline orientation as the angle between the geographic north and the line perpendicular to the linear regression fit.

For the model forcing, the model uses a single wave point. This defines the wave power and the incoming wave direction across the entire beach. The model assumes that the waves are homogeneous along the coast and assigns a single wave value to the whole beach by selecting a representative point beyond the active beach profile outside the closure depth (Hallermeier, 1977). Therefore, using a nearshore wave force inside the active beach profile would not be appropriate. Using a single wave point is a practical choice that simplifies computational complexity and minimises the need for extensive data collection. This approach enables the model to efficiently simulate shoreline rotation by focusing on the dominant wave conditions that drive sediment transport and beach morphology changes. It strikes a balance between model accuracy and computational efficiency, making it suitable for large-scale or long-term simulations where detailed spatial resolution is not as critical (Jaramillo et al., 2021).

It is essential to state that the model does not consider short-term processes such as beach cusp formation, alongshore variable bar welding, or rip current embayments (Splinter et al., 2014). Aside from shoreline orientation, it does not explicitly consider any physical beach features, such as the mean grain size or the length of the active beach profile. However, there is a relationship between the morphological beach parameters and the model parameters that specify the equilibrium state and the model velocity. Based on this, the beach's physical characteristics are estimated by comparing calibration parameter values at different sites.

Furthermore, the proposed model does not explicitly include any additional tidal range parameters; however, as Castelle et al. (2014) suggested that equilibrium shoreline evolution models can be applied to a range of elevation contours in the intertidal zone with satisfactory efficiency.

4.3. Model implementation

Several preprocessing steps were implemented before feeding the shoreline data into the model to ensure accuracy and consistency. The shoreline position data could originate from various sources, including remote sensing technologies such as video camera systems, aerial imagery, orthophotos, or satellites, and in situ field surveys like beach profile measurements and topo-bathymetric surveys. The initial step involved rectification and geo-referencing, which are crucial for achieving accurate measurements, particularly when using oblique images captured from video cameras and satellite images. This intricate process requires a deep understanding of the rectification geometry within the images (Jaramillo et al., 2021).

Once the data was rectified and geo-referenced, a fixed baseline was established to reference all shoreline positions. Cross-shore profiles were generated at regular intervals along this baseline to standardize shoreline measurements, ensuring consistency across the different datasets. The time-averaged dry beach width was then subtracted from all recorded shoreline positions to remove temporal fluctuations associated with short-term beach dynamics. The resulting data within a defined domain were then demeaned to achieve a normalised shoreline orientation.

The shoreline orientation (α_s) was determined by fitting a linear regression model to the normalised shoreline positions. In this context, orientation is defined as the angle between the geographic north and the line perpendicular to the regression fit, following the approach of (Harley et al., 2014; Turki et al., 2013a).

The next step involves applying the rotation model. This process encompasses determining the incident wave power (P), defining the equilibrium wave direction function (EWDF), and calibrating and validating the shoreline rotation model to ensure accurate parameterisation of variables a, b, L^-, and L^+ for shoreline evolution predictions.

4.4. Calibration method

The choice of parameters greatly influences the effectiveness and efficiency of an algorithm. In this study, the selected EBSEM has been applied using a global optimisation algorithm called the SCE-UA (shuffled complex evolution method) (Duan et al., 1992, 1993, 1994). This robust optimisation technique has been highly successful in calibrating hydrology models (Jiang et al., 2023; Rahnamay Naeini et al., 2019) and applies to a wide range of fields, particularly in mechanical engineering (Lobato et al., 2022) and building energy modelling (Yu et al., 2022).

The model calibration process begins by generating a population of potential parameter sets, which are then divided into smaller subgroups known as complexes. Within each complex, a simplex search is conducted, evaluating the model's performance using predefined loss functions such as the Nash-Sutcliffe coefficient (NSE) or Root-mean-square error (RMSE) for different parameter combinations.

The least-performing parameter set within each complex is replaced with a new one derived from the other sets, guiding the search towards better solutions. Information is periodically exchanged between the complexes to prevent them from becoming stuck in suboptimal regions. This iterative process continues until the algorithm converges, which occurs when a stopping criterion is met, such as reaching a maximum number of iterations or achieving a desired level of improvement in the objective function (Duan et al., 1993).

4.5. Model performance evaluation metrics

To assess the model's performance, the rotation model was examined using various loss functions, such as the root-mean-square error (RMSE), the Nash-Sutcliffe efficiency coefficient (NSE), and the Mielke Skill Score (λ), considering the complete dataset of observations during the designated monitoring period for each case study.

RMSE (Eq. (7)) measures the differences between the measured data and the values predicted by the model. Generally, the smaller the RMSE, the more accurate the model's prediction is compared to the measurement.

$$RMSE = \sqrt{\frac{\sum_{i=1}^{n}(X_i - Y_i)^2}{n}} \tag{7}$$

Where X_i and Y_i represent the ith simulated and observed value, respectively, for the constituent being evaluated and n is the total

number of samples.

NSE was also used to assess the model's skill (Eq. 8). It is a normalised indicator that determines the relative magnitude of residual variance and is compared to the measured data variance. The value can range from -∞ to 1. When NS equals 1, there is a perfect match between the model and the observed. When NS equals 0, the model result is equivalent to the mean of the observed value, and when less than 0, it indicates that the observed mean is a better predictor than the model, which indicates unacceptable performance (Moriasi et al., 2007; Nash and Sutcliffe, 1970).

$$NSE = 1 - \frac{\sum_{i=1}^{n}(Y_i - X_i)^2}{\sum_{i=1}^{n}(Y_i - \overline{Y})^2} \tag{8}$$

Where X_i and Y_i, represent the ith simulated and observed value, respectively, for the constituent being evaluated, while $\overline{Y}$ is the mean of the observed data for the constituent being evaluated, and n is the total number of the observations.

λ (Eq. 9) extends Pearson's correlation by incorporating the impact of bias. When no bias is present, λ is identical to the correlation coefficient; however, in the presence of bias, λ decreases proportionally to the bias magnitude (Duveiller et al., 2016). λ values range from 1, indicating a perfect simulation, to 0, representing no correlation.

$$\lambda = 1 - \frac{n^{-1}\sum_{i=0}^{n}(X_i - Y_i)^2}{\sigma_x^2 + \sigma_y^2 + (\overline{X} - \overline{Y})^2 + \kappa} \tag{9}$$

Here, X_i and Y_i represent the ith simulation and observed value and its value at each time step, respectively, while $\overline{X}$ and $\overline{Y}$ denote their means at each time step. σ_X and σ_Y are the standard deviations of the simulations and observations, respectively. The parameter κ (Eq. 10) depends on the Pearson correlation coefficient (R).

$$\kappa = \begin{cases} 0, & R \geq 0 \\ 2\left|\sum_{i=1}^{n}(X_i - \overline{X})(Y_i - \overline{Y})\right|, & R < 0 \end{cases} \tag{10}$$

5. Results

This section presents the performance of the selected EBSEM proposed by Jaramillo et al. (2021), also known as the JA21 model, in this study. These include model results from study sites using the complete time series of the observation data available (Section 5.1), model results when considering different data frequencies (Section 5.2), and model results considering observations at different contours (Section 5.3).

5.1. Model performance

This subsection presents the performance of the JA21 model when applied to the selected study sites using the observation dataset. The findings are summarised in Fig. 5 and Table 2, where each panel depicts results for specific locations: Narrabeen Beach (Fig. 5a), Tairua Beach (Fig. 5b), Poniente Beach (Fig. 5c), Llevant Beach (Fig. 5d), Cala Millor Beach (Fig. 5e), Moncofa Beach (Fig. 5f), and Blackpool Beach (Fig. 5g). In each panel, the red line represents the model results, while the grey dots represent the observed orientation data over the study period. Additionally, the box in each panel contains the model fitness scores (RMSE, λ, NSE) obtained from the comparison between the measurements and the model, along with their calibration parameters (L^+, L^-, a, b).

5.1.1. Narrabeen Beach

The performance of the JA21 model for Narrabeen Beach was evaluated from 1976 to 2019. The model accurately captured the general variability of shoreline rotation over this period (Fig. 5a). The observed variability was consistently captured within the model's 95 % confidence interval. However, it should be noted that the model adjusted better to the measurements from 1995 onward compared to the previous years while falling short in January 1990. Despite this occasional deviation, most observed data points remain within the confidence band.

The model's accuracy is reflected in the RMSE value of 0.23°, which indicates that the model's predicted shoreline orientations are in close agreement with the measured data with low error. The λ *value*, 0.82, also indicates a strong correlation between the model's predictions and observations, as a λ value above 0.7 indicates reliable model performance.

(Duveiller et al., 2016), highlighting the robustness of the model in simulating the observation. The NSE value of 0.70 further demonstrates the model's effectiveness, as it shows 70 % of the variance in the observation data, which is considered acceptable for results based on NSE thresholds for environmental modelling (Moriasi et al., 2007; Nash and Sutcliffe, 1970). The maximum variability of the shoreline orientation (α_m) recorded at Narrabeen Beach reached up to 1.96° throughout the study (Table 2), reflecting the dynamic nature of the beach.

5.1.2. Tairua Beach

The JA21 model's performance was assessed for Tairua Beach from 1999 to 2013. The results (Fig. 5b) show a good agreement with the measurement except for some specific short periods, winter 2004 and 2007, where the model could not accurately resolve the shoreline orientation, as these periods were when the rotation of the beach exceeded and was less than the average model speed, respectively. The model achieved an RMSE of 0.55°, indicating that the model predicted shoreline orientation is moderately close to the observed data with some deviations.

The λ value obtained was 0.81, signifying a strong agreement between the model predictions and the observations, as values above 0.7 indicate good model reliability. The NSE value of 0.62 also suggests that the models explain 62 % of the variance in the observation data, reflecting a reasonable performance. The α_m recorded at Tairua Beach over the study period is 5.15° (Table 2). Highlighting the significant changes in the rotational movement of the shoreline during the study period.

5.1.3. Poniente Beach

The performance of the JA21 model was evaluated for Poniente Beach after the nourishment activities on the beach from May 1991 to 2022. The model's results (Fig. 5c) show good agreement with the measurement by effectively reproducing the recovery process after the beach nourishment until equilibrium was reached in 2010 and continuing to perform well in subsequent years.

Quantitatively, the model achieved a RMSE of 0.18°, indicating a high level of accuracy in predicting the shoreline orientation compared to the observed data. The λ value was 0.94, demonstrating a robust correlation between the model's predictions and observations, with values approaching the maximum agreement. The NSE value of 0.89 also reflects the model's ability to explain 89 % of the variance in the observation data, which indicates the model's performance and reliability. The α_m recorded at Poniente Beach is 3.13°, highlighting significant but moderate rotational changes in the shoreline during the study period.

5.1.4. Llevant Beach

The JA21 model exhibits variable performance when applied to Llevant Beach (Fig. 5d) over the study period (1984–2022), which is also reflected in its wider confidence interval. For instance, the model demonstrated good agreement with the observed shoreline orientations from 1984 to 2005, capturing the rotational trends effectively. However, between 2005 and 2010, the model predictions consistently overestimated the observed shoreline orientation while maintaining the correct rotation trend.

The model achieved an RMSE of 0.26°, indicating a moderate devi-

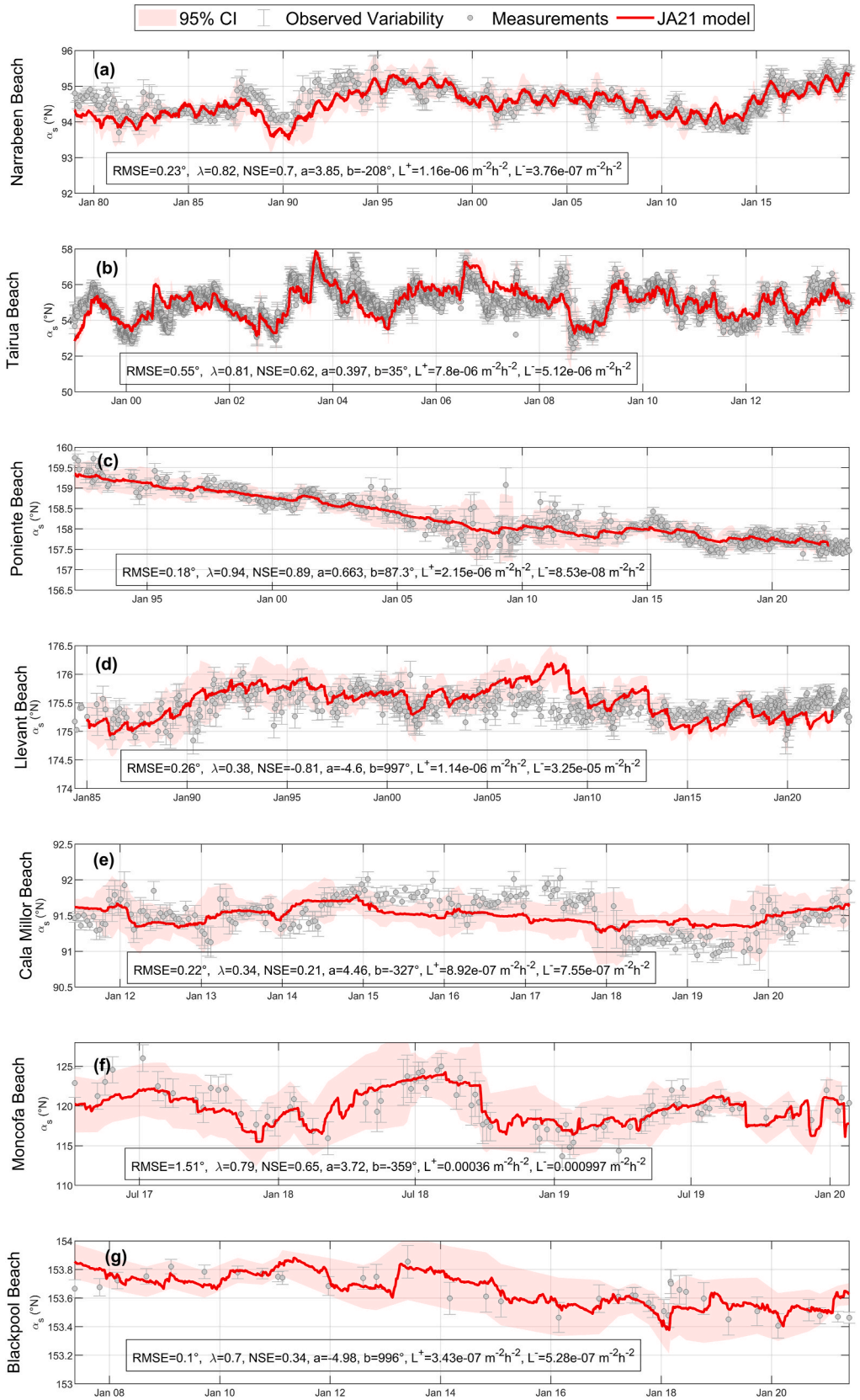

Fig. 5. *Model results of the shoreline orientation evolution model for (a) Narrabeen Beach, (b) Tairua Beach, (c) Poniente Beach, (d) Llevant Beach, (e) Cala Millor Beach, (f) Moncofa Beach, and (g) Blackpool Beach. The red line in each panel represents the modelled shoreline orientation, while the shaded region indicates the 95 % confidence interval. The observed shoreline orientations are shown as grey dots, with error bars denoting observed variability. The box in each panel provides the model performance metrics (RMSE, λ, NSE), along with their calibration parameters (L^+, L^-, a, b), derived from comparisons between the observed and modelled shoreline orientations.* (For interpretation of the references to colour in this figure legend, the reader is referred to the Web version of this article.)

Table 2
Summary of the quantitative statistics and calibration parameters for all selected study sites: root mean square error (RMSE), Mielke skill score (λ), Nash-Sutcliffe efficiency coefficient (NSE), proportionality constants corresponding to clockwise rotation (L^+), proportionality constants corresponding to counterclockwise rotation (L^-) slope coefficient (a), y-intercept (b), and maximum variability of the shoreline orientation (α_m).

	RMSE (°)	λ	NSE	L^+ ($m^{-2}h^{-2}$)	L^- ($m^{-2}h^{-2}$)	a	b (°)	α_m (°)
Narrabeen Beach	**0.23**	**0.82**	**0.70**	1.16E-06	3.76E-07	3.85	−207.00	1.96
Tairua Beach	**0.55**	**081**	**0.62**	7.80E-06	5.12E-06	0.40	35.00	5.15
Poniente Beach	**0.18**	**0.94**	**0.89**	2.15E-06	8.53E-08	0.66	87.30	3.13
Llevant Beach	0.26	0.38	−0.81	1.14E-06	3.25E-05	−4.60	997.00	0.90
Cala Millor Beach	0.22	0.34	0.24	8.92E-07	7.55E-07	4.46	−327.00	1.08
Moncofa Beach	**1.51**	**0.79**	**0.65**	3.60E-04	9.97E-04	3.72	−359.00	12.34
Blackpool Beach	**0.10**	**0.70**	0.34	3.43E-07	5.28E-07	−4.98	996.00	0.45

ation between the modelled and the observed shoreline orientations. The λ value of 0.38 suggests a weak agreement and limited correlation between the model's predictions and the measurement. Furthermore, the NSE value −0.81 highlights that the model performance is poor, with the model predictions performing worse than simply using the mean of the observed data. This negative NSE value indicates the model's inability to account for significant variability, particularly anthropogenic influences in the region. The α_m recorded for Llevant beach is 0.90° (Table 2), highlighting relatively low rotational dynamics compared to other study sites.

5.1.5. Cala Millor beach

The JA21 model demonstrated moderate performance in reproducing the shoreline orientation variability at Cala Millor Beach from 2011 to 2020 (Fig. 5e), with the measurements generally aligning with the model's confidence interval. The model predictions align reasonably well with the observed shoreline rotation trends from 2011 to 2015, effectively capturing the general variability over this interval. However, discrepancies between modelled and observed orientations were evident from 2015 onwards, reducing the model's accuracy.

Quantitative metrics further highlight these limitations. The model achieved an RMSE of 0.22°, reflecting moderate deviations between the model predictions and observations. The λ of 0.34 indicates weak agreement between the model prediction and measured data, emphasising a limited correlation. The NSE of 0.24 suggests that the model captures only 24 % variance in the observed data, highlighting its limited performance in representing the full range of variability. The α_m observed at Cala Millor Beach was 1.08°, pointing to relatively low rotational dynamics compared to other sites.

5.1.6. Moncofa Beach

The JA21 model demonstrated a good performance in reproducing the shoreline orientation variability at Moncofa Beach during the study period (Fig. 5f). The model effectively captured the general trends of shoreline rotation and showed better agreement when compared to the observation from July 2018 onwards.

The model achieved a RMSE of 1.51°, which can be attributed to the significant rotational dynamics recorded at Moncofa Beach with a α_m of 12.34°. The λ of 0.79 further indicates a strong correlation between the predictions and measurements. Additionally, the NSE value of 0.65 highlights that the model accounts for 65 % of the variance in the observation data, a performance considered acceptable based on the standard NSE thresholds. Overall, the statistical results suggest a satisfactory agreement between the model predictions and the observed values.

5.1.7. Blackpool Beach

The JA21 model demonstrated a good performance in reproducing the shoreline orientation variability at Blackpool Beach during the study period (Fig. 5g), with the observed variability comparatively low and consistently fitting with the confidence band. The model successfully captured the overall trends in shoreline orientation, aligning reasonably well with observed data across most periods. However, there were exceptions. For instance, no observation data was recorded in 2011, making it impossible to evaluate model performance for that year. Additionally, during the winter of 2014, the model struggled to resolve the shoreline accurately as the rate of beach rotation exceeded the model's average predictive capability.

The model achieved a RMSE of 0.10°, indicating a good alignment between the modelled and observations. The λ of 0.70 reflects a moderate correlation between the model predictions and measurements. However, the NSE value of 0.34 indicates that the model captures only 34 % of the variance in the observed data, which is modest. The α_m recorded at Blackpool Beach was 0.45°, which is relatively low compared to other study sites, highlighting the limited rotational dynamics observed at the beach.

Table 2 further summarises the quantitative statistics, calibration parameters, and maximum degree of shoreline orientation obtained from all study sites. The maximum degree of shoreline refers to the difference between the degree of the most clockwise shoreline orientation and the degree of the most counterclockwise orientation. This value is denoted by α_m.

5.2. Model sensitivity to temporal resolution

The performance of the JA21 model was evaluated using three data frequencies, daily, weekly, and monthly, at Tairua Beach to assess its sensitivity to temporal resolution. The primary objective of this analysis is to ascertain whether the data frequency impacts the model's performance in reproducing shoreline orientation variability.

The results (Fig. 6a–c) show that the JA21 model can consistently and effectively capture the shoreline orientation variability across different data frequencies with minimal degradation in accuracy. The RMSE values remain steady between 0.54° and 0.55°, signifying that the model's predictive accuracy is robust and largely unaffected by changes in data resolution. The performance metrics, such as the λ and NSE values, decrease slightly as the data frequency decreases. For daily data frequencies, the values are λ = 0.81 and NSE = 0.62. These values slightly decrease to λ = 0.80 and NSE = 0.61 for weekly data frequencies and to λ = 0.78 and NSE = 0.56 for monthly data frequencies.

Additionally, as the data frequency decreases from daily to monthly, the model parameters ('*a*' and '*b*') show minor variations. For instance, parameter '*a*' increases from 0.397 (daily) to 0.468 (monthly), while parameter 'b' decreases from 35° to 31°. This trend reflects a smoothing effect as the data frequency decreases, reducing short-term variability in shoreline dynamics. Similarly, the proportionality constants also vary, indicating that the model responds to temporal scales differently.

5.3. Model sensitivity across shoreline elevation contours

Building on the suggestion of Castelle et al. (2014), EBSEMs can be effectively applied to various elevation contours within the intertidal zone with satisfactory efficiency. This study assesses the capability of the JA21 model in reproducing shoreline rotation variability at four distinct elevation contours (−0.5 m, 0 m, 1.0 m, and 2.0 m) at Narrabeen Beach, a microtidal sandy beach with high-frequency monitoring, and

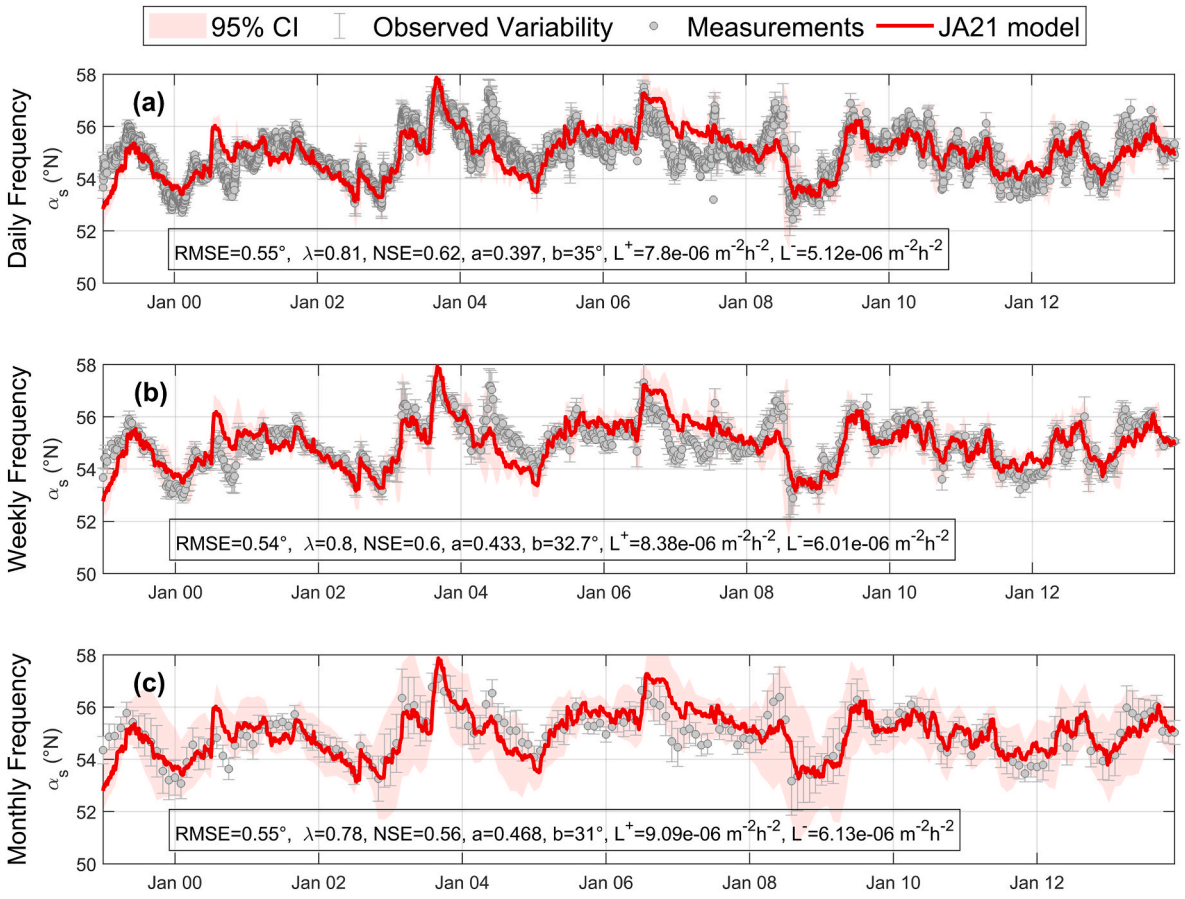

Fig. 6. Model results for Tairua Beach using different data frequencies: (a) Daily frequency, (b) Weekly frequency, (c) Monthly frequency. The red line in each panel represents the modelled shoreline orientation, while the shaded region indicates the 95 % confidence interval. The observed shoreline orientations are shown as grey dots, with error bars denoting observed variability. The box in each panel provides the model performance metrics (RMSE, λ, NSE), along with their calibration parameters (L^+, L^-, a, b), derived from comparisons between the observed and modelled shoreline orientations. (For interpretation of the references to colour in this figure legend, the reader is referred to the Web version of this article.)

Blackpool Beach, a macrotidal gravel beach with low-frequency monitoring. The comparative analysis of these two distinct coastal environments provides more insights into the model's robustness and applicability across different hydrodynamics and sedimentary conditions.

At Narrabeen Beach, the JA21 model effectively captures shoreline orientation variability with a high level of consistency across all elevation contours (Fig. 7a–d). However, variability in model performance is observed across different intertidal elevations. The RMSE values range from 0.20° to 0.28°, with contour −0.5m having the highest RMSE. This suggests that model predictions deviate slightly more from observed orientations at lower intertidal regions, where increased wave forcing and sediment mobility introduce higher uncertainty in shoreline position predictions. The λ remains consistently high (≥0.75) across all the contours, signifying a strong correlation between the model predictions and the observed data. The NSE values ranging from 0.61 to 0.71 further support the model's reliability in reproducing the observed shoreline variability with the best performance observed at the 1.0 m and 2.0 m contours, where the influence of hydrodynamic processes is reduced, leading to more stable shoreline configurations. The calibration parameters L^+ and L^- exhibit considerable variation across contours, reflecting differences in sediment redistribution due to tidal and wave-driven processes. The most significant rotational response was observed at the lower intertidal zones, where the model had to account for increased cross-shore sediment transport.

Despite Blackpool Beach's macrotidal regime and lower temporal resolution of shoreline monitoring, the model exhibits strong predictive performance across all elevation contours (Fig. 7e–h). The RMSE value remains relatively low (0.07°–0.10°), indicating good agreement between the modelled and observed shoreline orientation. The λ increases from 0.65 at −0.5 m to 0.84 at 2.0 m, suggesting that shoreline rotation becomes more predictable at higher elevations due to lower hydrodynamic variability. Similarly, the NSE values range from 0.23 at −0.5 m to 0.65 at 2.0 m, reflecting the improved predictive capability of the model at higher elevations. The L^+ and L^- values vary across elevation levels, with higher values at lower elevations, indicating increased sensitivity of shoreline rotation to wave action at −0.5 m and 0 m contours.

Overall, the results demonstrate that the JA21 model effectively simulates shoreline rotation across a diverse range of coastal environments, temporal scales, and elevation contours. Performance varied depending on beach type, data resolution, and elevation contours, revealing distinct behavioural patterns and sensitivities. These findings form the basis for further examination of the model skill, parameter variability, and sensitivity in the following discussion section.

6. Discussion

The results presented in Section 5 demonstrate the ability of the JA21 model to replicate the evolution of shoreline orientation variability across seven beaches worldwide: Narrabeen Beach, Tairua Beach, Poniente Beach, Llevant Beach, Cala Millor Beach, Moncofa Beach, and Blackpool Beach. These study sites exhibit diverse physical and environmental characteristics, as outlined in Table 1, including a range of

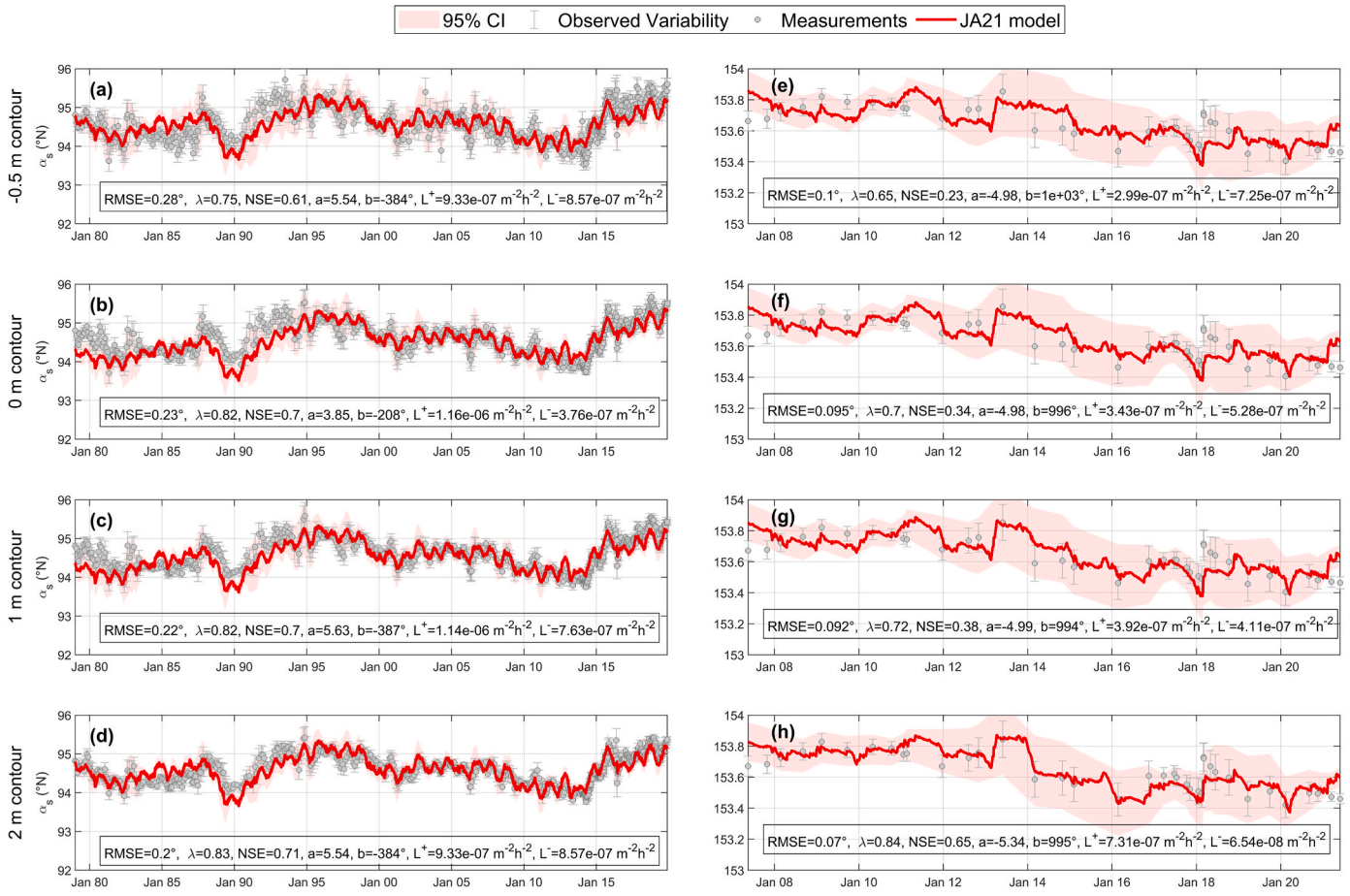

Fig. 7. Model results across different elevation contours for (a–d) Narrabeen Beach and (e–h) Blackpool Beach at −0.5 m, 0 m, 1 m, and 2 m elevation contours. The red line in each panel represents the modelled shoreline orientation, while the shaded region indicates the 95 % confidence interval. The observed shoreline orientations are shown as grey dots, with error bars denoting observed variability. The box in each panel provides the model performance metrics (RMSE, λ, NSE), along with their calibration parameters (L^+, L^-, a, b), derived from comparisons between the observed and modelled shoreline orientations. (For interpretation of the references to colour in this figure legend, the reader is referred to the Web version of this article.)

sediment types (sandy to gravel), tidal regimes (microtidal to macrotidal), beach lengths (from hundreds of meters to several kilometers), and varying data collection methods (field surveys, video monitoring, and satellite imagery). Additionally, the temporal resolution of available datasets varies from daily monitoring to six-monthly observations.

Evaluating the performance of this EBSEM for rotation movement across such a broad spectrum of coastal settings is crucial, as prior studies have been carried out on a handful of case studies of microtidal sandy beaches. For example (Turki et al., 2013a), analysed three small pocket sandy beaches (Bogatell, Nova Icaria, and Somorrostro) in Barcelona, Spain, while (Blossier et al., 2017) applied the model to Tairua Beach (Jaramillo et al., 2021). extended its application to Narrabeen and Tairua Beach. However, the diversity of beaches investigated in this study, particularly those characterised by gravel substrates or macrotidal environments, expands the range of conditions under which the model has been validated, thereby enhancing the model's applicability in global coastal management efforts.

6.1. Model skill and performance evaluation

The JA21 model demonstrates robust performance in replicating shoreline orientation variability across a range of coastal environments, as evidenced by strong correlations between modelled and observed data. The performance metrics (RMSE, λ, and NSE) consistently indicate high reliability across most sites (Section 4; Table 2). For instance, the magnitude of the RMSE between the modelled and measured shoreline orientations for Narrabeen Beach, Poniente Beach, Llevant Beach, Cala Millor Beach, and Blackpool Beach remains relatively low, highlighting the model's ability to track observed trends closely. However, sites like Tairua Beach and Moncofa Beach exhibit high RMSE values. These high values can be attributed to the significant variability of the shoreline orientation of these locations, with Tairua Beach reaching a maximum shoreline orientation variability of 5.15° and Moncofa Beach reaching 12.34°.

Nevertheless, the model's performance, even under these conditions, aligns with the criteria outlined by (Moriasi et al., 2007; Nash and Sutcliffe, 1970), which considers simulations satisfactory when NSE >0.50. Notably, the NSE values across most sites meet or exceed this threshold, supported by the consistently high λ values across all study sites, reinforcing the model's ability to reproduce shoreline orientation. However, exceptions at Llevant Beach and Cala Millor Beach highlight areas where specific environmental or data-related challenges influence the model's predictive ability.

At Llevant Beach, the weak performance of the model can be linked to the fact that the maximum shoreline orientation is less than one degree, which introduces a high level of uncertainty. Furthermore, the source data for Llevant Beach was derived from satellite imagery, particularly before 2015, when Landsat imagery was available at a 30 m resolution and is also characterised by considerable uncertainty. Between 2005 and 2010, the model's predictions exceeded the actual measurements. This discrepancy can be attributed to a significant decrease in average storm duration during that period (Toledo et al.,

2022), a factor that the model could not incorporate. Nevertheless, the model still managed to capture the overall rotation trend observed on the beach.

For Cala Millor Beach, the model's difficulties in replicating the beach orientation variation can be attributed to the natural variability of the nearby *Posidonia Oceanica* seagrass beds, known for influencing sediment dynamics (Abreu et al., 2020), which is not captured by the model forcing. Additionally, human interventions, such as sediment redistribution by local municipalities as part of coastal management strategies, introduce variability that the model cannot predict.

It is worth noting that the results for Narrabeen Beach and Tairua Beach in this study show minor differences compared to the findings of Jaramillo et al. (2021). These discrepancies can be attributed to differences in calibration methodologies and the availability of extended datasets. For instance, this study incorporates observations for Narrabeen Beach up to 2019, whereas the earlier analysis by Jaramillo et al. (2021) covered data only until 2015. Despite these variations, the performance of the JA21 model in reproducing shoreline orientation variability has consistently demonstrated high accuracy and reliability across all datasets.

In terms of rotation speed, Moncofa Beach and Tairua Beach exhibit faster shoreline rotation rates compared to other beaches, as evidenced by the parameters L^+ and L^-, which quantifies clockwise and counterclockwise rotational speeds, respectively. Moncofa Beach's higher rotation speed can be attributed to its relatively small length (330 m) despite its coarse sediment size ($D_{50} > 4.0$ mm), consistent with Turki et al. (2013b) findings that smaller beaches or smaller sediment size beaches tend to rotate more rapidly due to reduced alongshore transport distance. In contrast, Tairua Beach, the shortest sandy beach in the dataset (1 200 m), also exhibits rapid rotation, influenced by both its fine sediment ($D_{50} > 0.45$ mm), and limited beach length, which enhances responsiveness to external forcing.

Interestingly, Blackpool Beach displays a slow rotational response despite its short length (650 m), a result of its macrotidal environment and coarse sediment ($D_{50} > 5.0$ mm), which dampens shoreline movement by reducing sediment mobility. This highlights the combined influence of tidal range, sediment size, and beach length on rotation dynamics. On the other hand, beaches like Narrabeen Beach and Poniente Beach, characterised by medium sediment sizes and greater lengths (3 600 m and 3 008 m, respectively), exhibit slower rotation responses occurring over seasonal to interannual timescales, with fewer rapid fluctuations. These results highlight the importance of sediment properties and morphodynamic settings in determining shoreline orientation changes' temporal and spatial scales across diverse coastal systems.

The rotational variability observed on Moncofa and Tairua Beaches is further influenced by storm events and seasonal variations, with changes evident over shorter timescales (days to weeks and months). In contrast, the rotational movements on Narrabeen and Poniente Beaches are primarily shaped by long-term sediment transport and wave climate variability, with fluctuations occurring between seasonal and interannual time scales.

6.2. Variability in calibration parameters

The calibration parameters of the EBSEM show substantial variability across the studied sites, reflecting the unique hydrodynamic forces, sediment dynamics, and morphological responses specific to each location.

The L^+ values ranged from 3.43×10^{-7} $m^{-2}h^{-2}$ at Blackpool Beach to 3.60×10^{-4} $m^{-2}h^{-2}$ at Moncofa Beach. The higher values observed at beaches such as Moncofa indicate increased sensitivity to clockwise rotation, likely driven by wave-induced sediment transport processes. In contrast, lower values at Blackpool Beach indicate a more stable shoreline orientation under wave-forcing conditions. Similarly, the L^- values varied across study sites, with values ranging from 8.53×10^{-8} $m^{-2}h^{-2}$ at Poniente to 9.97×10^{-4} $m^{-2}h^{-2}$ at Moncofa Beach. The high L^- at Moncofa Beach reflect pronounced shoreline rotation due to asymmetrical wave exposure and sediment dynamics. In contrast, beaches such as Poniente exhibit lower values, signifying reduced counterclockwise rotational responses.

The slope coefficient (a), which characterises the relationship between the wave forcing and shoreline orientation changes, showed both positive and negative trends. The positive values at sites like Poniente indicate a direct correlation between wave forcing and rotational response. In contrast, negative values at sites like Blackpool and Llevant indicate complex interactions among incident wave forcing, sediment supply variability, and morphological feedback processes that diverge from direct linear relationships. The intercept coefficient (b), indicative of the reference shoreline orientation, also displayed significant variation, from −359° at Moncofa Beach to approximately 997° at Llevant Beach, emphasising the site-specific nature of shoreline equilibrium states.

Overall, this variability in EBSEM calibration parameters highlights the need for site-specific calibration when applying shoreline rotation models in engineering applications. Improved parameterisation, particularly at beaches exhibiting high rotational sensitivity, could significantly improve model predictions, thus enabling more informed coastal management decisions. It is crucial to account for the distinct wave-sediment-morphology interactions observed at each site to enhance predictive accuracy and bolster the reliability of shoreline rotation models in coastal management practices.

6.3. Model sensitivity to temporal resolution and elevation contours

Analysing the JA21 model to temporal resolution reveals its robustness in capturing shoreline variability across daily, weekly, and monthly data frequencies. Despite slight variations in model performance metrics, the results indicate minimal degradation in accuracy as the temporal resolution decreases. The RMSE values, which remain within a narrow range of 0.54°–0.55°, highlight the model's consistent predictive accuracy. However, metrics such as λ and NSE exhibit a marginal decline from 0.81 to 0.62, respectively, for daily data to 0.78 and 0.56 for monthly data. This decline suggests that while the JA21 model effectively reproduces long-term shoreline trends, short-term variability may become smoothed as the temporal resolution decreases. Furthermore, the empirical parameters 'a' and 'b' slightly decrease with longer averaging periods, indicating reduced variability and a more smoothed response to the beach orientation. The calibration parameters L^+ and L^- also vary, reflecting the changes in the forcing at different temporal scales.

A Q-Q (quantile-quantile) plot was employed to understand further if the measured data from each frequency is generally consistent with the theoretical normal distribution. The analysis of the results, as illustrated in Fig. 8a–c, indicates a strong alignment between the blue cross symbols representing the measurements and the red dashed line representing the model. This alignment suggests a reasonable agreement between the model and the observed data, indicating that the model effectively captures the general distribution of the measurements. However, there are noticeable deviations at the distribution's lower and upper ends. These deviations suggest that while most of the data follows a normal distribution, outliers may be present or a slight skew in the data, especially in the distribution's tails.

Upon closer examination of the daily data frequencies (Fig. 8a), it is evident that the model demonstrates a slightly better fit with the measurements, indicating that it is more effective at capturing the daily variations in the data than other frequencies. The agreement between the model and measurements remains strong for the weekly data frequencies (Fig. 8b), although there is a slight deviation in the upper quantiles. This suggests that the model might underestimate the extreme values in the weekly data. Lastly, when considering the monthly data frequencies (Fig. 8c), the model still shows a reasonable agreement with

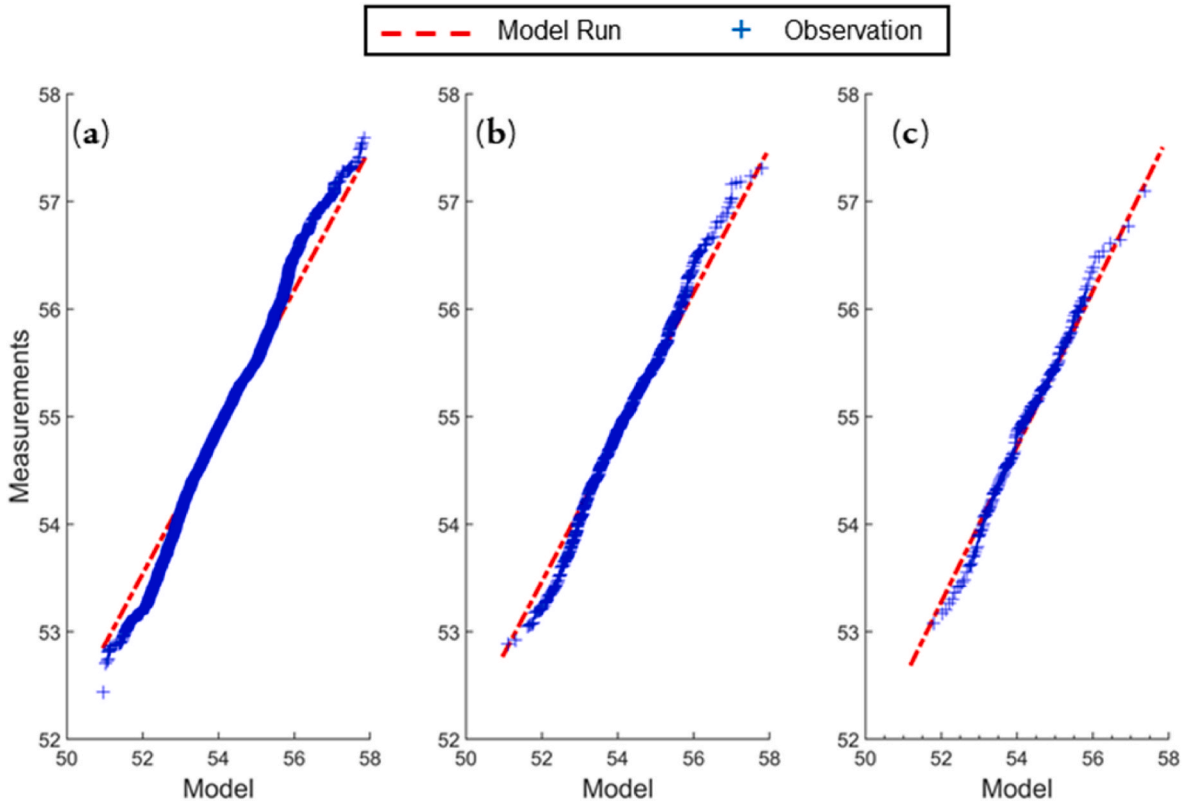

Fig. 8. Quantile-quantile (Q–Q) plots of measurement against model data considering different data frequencies. The red broken line represents the model run, while the cross sign represents the observation of (a) Daily frequencies, (b) Weekly frequencies, and (c) Monthly frequencies. (For interpretation of the references to colour in this figure legend, the reader is referred to the Web version of this article.)

the measurements. However, a more pronounced deviation in the upper quantiles indicates that the model might face challenges in accurately capturing the extreme values in the monthly data.

The JA21 model demonstrates strong and consistent performance in simulating shoreline orientation across various elevation contours under differing intertidal conditions. The statistical metrics obtained at Narrabeen Beach and Blackpool Beach, presented in subsection 5.3 and Fig. 7, highlight the influence of elevation-dependent hydrodynamic processes on model performance. Notably, lower elevation contours (−0.5 m and 0 m) exhibit more significant wave-driven variability, reflected in the wider confidence intervals, indicating increased uncertainty in model predictions. This increased variability is attributed to the stronger hydrodynamic forcing and sediment transport processes in the lower intertidal zone. In contrast, higher elevation contours (1.0 m and 2.0 m) demonstrate more stable shoreline orientations, with reduced variability and improved model accuracy, as evidenced by the higher NSE and λ values (Moriasi et al., 2007; Nash and Sutcliffe, 1970). These results confirm the model's ability to capture elevation-dependent shoreline rotation dynamics across both microtidal sandy and macrotidal gravelly environments.

The sensitivity of L^+ and L^- parameters across elevation contours further highlights the influence of intertidal hydrodynamics on sediment redistribution. The results indicate higher rotational sensitivity in lower intertidal areas, where short-term shoreline fluctuations are more pronounced due to wave and tidal influences. This aligns with previous studies emphasising more significant morphological variability in lower intertidal regions compared to more stable upper beach zones (Harley et al., 2011a). Furthermore, differences in sediment composition between Narrabeen Beach and Blackpool Beach contribute to site-specific variations in model performance, reinforcing the necessity of localised calibration when applying shoreline evolution models.

The observed variations in model skill scores and calibration parameters across elevation contours suggest that intertidal dynamics strongly influence shoreline rotation, with lower elevations (−0.5 m and 0 m) exhibiting more significant wave-driven variability. This increased variability is evident in the wider confidence intervals at these contours, suggesting more substantial uncertainty in model predictions. Conversely, higher elevation contours (1.0 m and 2.0 m) show more stabilised responses due to reduced hydrodynamic forcing, leading to reduced variability and improved model accuracy. Hence, the JA21 model effectively captures these contour-dependent dynamics in both microtidal (sandy) and macrotidal (gravelly) environments, as evidenced by the NSE and λ values (Moriasi et al., 2007; Nash and Sutcliffe, 1970).

However, parameter sensitivity differs based on sediment composition and hydrodynamic forcing. The L^+ and L^- parameters exhibited contour-dependent variations, reflecting differences in sediment redistribution across intertidal zones. Higher rotational sensitivity was observed in the lower intertidal areas, where short-term shoreline fluctuations due to tidal and wave-induced sediment transport are more pronounced. These findings align with previous studies that emphasise the more significant morphological variability of lower intertidal regions compared to upper beach zones (Harley et al., 2011a).

These findings demonstrate the JA21 model's adaptability to elevation-specific shoreline dynamics and highlight the importance of considering intertidal variability in shoreline evolution modelling. The observed performance variations across elevation contours emphasise the need for site-specific parameterisation in predictive models of coastal morphodynamics, particularly in environments where tidal range, sediment composition, and wave energy significantly influence shoreline stability.

6.4. Model uncertainties and limitations

The JA21 model, while demonstrating robust performance consistently across diverse coastal settings, has certain limitations that highlight areas for potential refinement. One key source of uncertainty stems from the variability in input datasets' accuracy, including satellite imagery, video monitoring, and in-situ field surveys. For example, field survey data, such as those collected at Narrabeen Beach, provide the highest accuracy, as evidenced by the minimal dispersion observed in the measurements (Fig. 5a), unlike satellite-derived datasets, which offer extensive temporal and spatial coverage but are limited by their resolution, particularly for small-scale rotational dynamics. For instance, Landsat imagery (30 m resolution) was used for Poniente, Llevant, and Moncofa beaches before 2015 and Sentinel imagery (10 m resolution) available from 2015 onward (Acker et al., 2003; Payra et al., 2023).

The model's sensitivity to the temporal resolution of input data presents another limitation. High-frequency monitoring, such as the daily data collected at Tairua Beach, produces more accurate predictions than low-frequency datasets, such as the six-monthly intervals used at Blackpool Beach. This reliance on temporal resolution may restrict the model's applicability in regions where consistent, high-resolution data are unavailable, potentially affecting its accuracy.

Additionally, the model calibration parameters (a, b, L^+, and L^-), calibrated based on historical data, are effective under normal conditions but struggle with nonlinear processes like abrupt morphological changes induced by extreme events. This limitation is particularly evident in environments with high variability, such as Moncofa Beach during the winter of 2014, where storm-induced changes challenge the model's assumptions as the beach rotation exceeds the model's predictive capability. Similarly, in Poniente Beach, the model could not capture the disequilibrium caused by the massive nourishment on the beach in May 1991 (Toledo et al., 2022). Nevertheless, the model successfully reproduced sediment diffusion, showing beach rotation until reaching equilibrium.

7. Conclusions

This study evaluated the performance of the EBSEMs in simulating the shoreline rotation variability across diverse characteristics, including sediment types, tidal ranges, monitoring frequency, data sources, and beach lengths. Analysing Narrabeen Beach, Tairua Beach, Poniente Beach, Llevant Beach, Cala Millor Beach, Moncofa Beach, and Blackpool Beach broadens the scope of EBSEMs as previous studies have primarily focused on a handful of microtidal sandy beaches. Based on the research findings, the following conclusions were drawn.

The JA21 model demonstrated satisfactory skills in reproducing the rotational variability of shorelines across various beach types. Quantitative statistics highlighted satisfactory model performance, with metrics such as root-mean-square error, the Nash-Sutcliffe coefficient, and the Mielke Skill Score across the studied sites indicating strong model alignment with observed rotation patterns. Seasonal rotation trends were evident, with clockwise rotation occurring from summer to winter and counterclockwise from winter to summer, notably over shorter time scales at Tairua, Cala Millor, Moncofa, and Blackpool beaches due to storm events and seasonal shifts. Longer-term rotation patterns were observed at Narrabeen, Poniente, and Llevant beaches, demonstrating EBSEM's applicability across short- and long-term temporal scales.

Despite the model's robust performance, it encountered difficulties in accurately replicating shoreline changes influenced by natural and anthropogenic factors. For instance, fluctuations in storm intensity at Llevant Beach between 2005 and 2010 revealed limitations in EBSEM's responsiveness to episodic events. Additionally, human interventions impacted model accuracy, as observed at Poniente and Cala Millor beaches. Morphological parameters such as beach length and sediment size also influenced rotation speeds, with shorter beaches and finer sediments rotating more rapidly than more extended beaches or those with coarser sediment, highlighting a need for parameter refinements.

While the JA21 model has proven effective in numerous settings, opportunities for further model improvements remain. Addressing systematic biases and refining parameters to better account for beach-specific characteristics, anthropogenic activities, and storm-induced shoreline variability could improve scalability and precision, enabling broader global application. These developments would enhance the model's ability to support coastal management initiatives by providing accurate, location-sensitive insights into shoreline dynamics.

The EBSEM model has practical applications in coastal management, supporting shoreline adaptation (e.g., beach nourishment, managed retreat) and hazard mitigation (e.g., seawalls, breakwaters) by predicting vulnerability and erosion-prone areas. Its scalability across diverse beach types makes it a valuable tool for assessing climate change impacts, such as rising sea levels and storm patterns. It informs evidence-based policies like setback lines and zoning regulations to balance development with coastal preservation.

Hence, these conclusions emphasise the potential for EBSEM to advance our understanding of coastal processes across diverse settings and support evidence-based decision-making in shoreline management and planning. By bridging the gap between theoretical modelling and practical applications, the JA21 model can contribute to the resilience of coastal communities and ecosystems in the face of natural and anthropogenic challenges.

CRediT authorship contribution statement

Mayowa Basit Abdulsalam: Writing – review & editing, Writing – original draft, Visualization, Validation, Software, Resources, Project administration, Methodology, Investigation, Formal analysis, Data curation, Conceptualization. **Camilo Jaramillo:** Writing – review & editing, Visualization, Validation, Supervision, Resources, Project administration, Methodology, Investigation, Data curation, Conceptualization. **Lucas de Freitas:** Writing – review & editing, Visualization, Software, Project administration, Methodology, Formal analysis. **Mauricio González:** Writing – review & editing, Validation, Supervision, Resources, Project administration, Conceptualization. **José A.Á. Antolínez:** Writing – review & editing, Visualization, Validation, Supervision, Project administration, Conceptualization.

Data and software availability

Most of the data used in this study were obtained from open-source repositories and relevant public archives. Specifically, datasets for Narrabeen-Collaroy Beach at http://narrabeen.wrl.unsw.edu.au, Tairua Beach at https://coastalhub.science/data, Cala Millor Beach at https://doi.org/10.25704/ahjv-da25, and Blackpool Beach at https://southwest.coastalmonitoring.org/. In contrast, the data for Moncofa Beach, Poniente Beach, and Llevant Beach are not publicly available; however, these datasets can be provided upon request. The JA21 EBSEM is available on GitHub at https://github.com/IHCantabria/IHSetJaramillo21a.

Declaration of competing interest

The authors declare that they have no known competing financial interests or personal relationships that could have appeared to influence the work reported in this paper.

Acknowledgements

The authors acknowledge the support of the Regional Ministry of Universities, Equality, Culture and Sports of the Government of Cantabria (Contract-Program between the Government of Cantabria and the University of Cantabria) under Grant PID2021-127994OB-I00

FutureBeach Project and the ThinkInAzul programme supported by MCIN/Ministerio de Ciencia e Innovación with funding from European Union NextGeneration EU (PRTR-C17.I1) and by Comunidad de Cantabria.

Additionally, we particularly appreciate the immense contributions of the Geo-Environmental Cartography and the Remote Sensing Group (CGAT) at the Polytechnic University of Valencia (UPV), the Narrabeen-Collaroy monitoring program, the Balearic Islands Coastal Observing and Forecasting System, the 5th Earth Observation Envelope Program (EOEP-5) of the European Space Agency, South West Coastal Monitoring Program and the University of Auckland for generously providing the diverse datasets that were utilised in this research.

C.J. has been supported by a Margarita Salas post-doctoral fellowship funded by the European Union-NextGenerationEU, Ministry of Universities and Recovery and Resilience Facility, through a call from the University of Cantabria.

References

Abreu, T., Parreño-Mas, B., Pinto-Faria, J., 2020. Coastal management risk analysis of an embayed beach in Majorca island. SN Appl. Sci. 2. https://doi.org/10.1007/s42452-020-03325-6.

Acker, J., Williams, R., Chiu, L., Ardanuy, P., Miller, S., Schueler, C., Vachon, P.W., Manore, M., 2003. Remote sensing from satellites. In: Meyers, R.A. (Ed.), Encyclopedia of Physical Science and Technology, third ed. Academic Press, New York, pp. 161–202. https://doi.org/10.1016/B0-12-227410-5/00938-8.

Almar, R., Coco, G., Bryan, K.R., Huntley, D.A., Short, A.D., Senechal, N., 2008. Video observations of beach cusp morphodynamics. Mar. Geol. 254, 216–223. https://doi.org/10.1016/j.margeo.2008.05.008.

Amores, A., Marcos, M., Carrió, D.S., Gómez-Pujol, L., 2020. Coastal impacts of storm gloria (January 2020) over the north-western mediterranean. Nat. Hazards Earth Syst. Sci. 20, 1955–1968. https://doi.org/10.5194/nhess-20-1955-2020.

Antolínez, J.A.A., Méndez, F.J., Anderson, D., Ruggiero, P., Kaminsky, G.M., 2019. Predicting climate-driven coastlines with a simple and efficient multiscale model. J Geophys Res Earth Surf 124, 1596–1624. https://doi.org/10.1029/2018JF004790.

Aragonés, L., García-Barba, J., García-Bleda, E., López, I., Serra, J.C., 2015. Beach nourishment impact on Posidonia oceanica: case study of Poniente beach (Benidorm, Spain). Ocean Eng. 107, 1–12. https://doi.org/10.1016/j.oceaneng.2015.07.005.

Azorakos, G., Castelle, B., Marieu, V., Idier, D., 2024. Satellite-derived equilibrium shoreline modelling at a high-energy meso-macrotidal beach. Coast. Eng. 191, 104536. https://doi.org/10.1016/j.coastaleng.2024.104536.

Black, Kerry Peter, Bryan, Karin R., Bogle, J.A., Bryan, K.R., Black, K.P., Hume, T.M., Healy, T.R., 2016. Video Observations of Rip Formation and Evolution.

Blossier, B., Bryan, K.R., Daly, C.J., Winter, C., 2017. Shore and bar cross-shore migration, rotation, and breathing processes at an embayed beach. J Geophys Res Earth Surf 122, 1745–1770. https://doi.org/10.1002/2017JF004227.

Bryan, K.R., Foster, R., MacDonald, I., 2013. Beach rotation at two adjacent headland-enclosed beaches. J. Coast Res. 165, 2095–2100. https://doi.org/10.2112/si65-354.1.

Castelle, B., Bujan, S., Marieu, V., Ferreira, S., 2020. 16 years of topographic surveys of rip-channelled high-energy meso-macrotidal sandy beach. Sci. Data 7. https://doi.org/10.1038/s41597-020-00750-5.

Castelle, B., Marieu, V., Bujan, S., Ferreira, S., Parisot, J.P., Capo, S., Sénéchal, N., Chouzenoux, T., 2014. Equilibrium shoreline modelling of a high-energy meso-macrotidal multiple-barred beach. Mar. Geol. 347, 85–94. https://doi.org/10.1016/j.margeo.2013.11.003.

Chadwick, A.J., Karunarathna, H., Gehrels, W.R., Massey Bsc, A.C., Dales, D., 2005. A New Analysis of the Slapton Barrier Beach System, UK.

Creel, L., 2003. Ripple effects: population and coastal regions. Population reference bureau Washington, DC.

D'Anna, M., Vitousek, S., Castelle, B., Idier, D., Ribas, F., Falqués, A., Coco, G., Yates, M., Le Cozannet, G., 2024. Reshaping the understanding of beach response to sea-level rise for equilibrium shoreline modelling. https://doi.org/10.4995/GEOLIT24.2024.18667.

Davidson, M.A., Splinter, K.D., Turner, I.L., 2013. A simple equilibrium model for predicting shoreline change. Coast. Eng. 73, 191–202. https://doi.org/10.1016/j.coastaleng.2012.11.002.

Davidson, M.A., Turner, I.L., 2009. A behavioral template beach profile model for predicting seasonal to interannual shoreline evolution. J Geophys Res Earth Surf 114. https://doi.org/10.1029/2007JF000888.

de Vriend, H.J., Zyserman, J., Nicholson, J., Roelvink, J.A., Péchon, P., Southgate, H.N., 1993. Medium-term 2DH coastal area modelling. Coast. Eng. 21, 193–224. https://doi.org/10.1016/0378-3839(93)90050-I.

Duan, Q., Sorooshian, S., Gupta, V., 1992. Effective and efficient global optimization for conceptual rainfall-runoff models. Water Resour. Res. 28, 1015–1031. https://doi.org/10.1029/91WR02985.

Duan, Q., Sorooshian, S., Gupta, V.K., 1994. Optimal use of the SCE-UA global optimization method for calibrating watershed models. J. Hydrol. Elsevier J. Hydrology 158 (1).

Duan, Q.Y., Gupta, V.K., Sorooshian, A.S., Dixon, L.C.W., 1993. Shuffled complex evolution approach for-e • o • effective and efficient global minimization. J. Optim. Theor. Appl. 76 (3).

Duveiller, G., Fasbender, D., Meroni, M., 2016. Revisiting the concept of a symmetric index of agreement for continuous datasets. Sci. Rep. 6, 19401. https://doi.org/10.1038/srep19401.

Ecolevante, 2006. Estudio Ecocartografico Del Litoral de Las Provincias de Alicante y Valencia. General Service of Coasts of the State. Madrid.

Enríquez, A.R., Marcos, M., Álvarez-Ellacuría, A., Orfila, A., Gomis, D., 2017. Changes in beach shoreline due to sea level rise and waves under climate change scenarios: application to the Balearic Islands (western Mediterranean). Nat. Hazards Earth Syst. Sci. 17, 1075–1089. https://doi.org/10.5194/nhess-17-1075-2017.

Fernández-Mora, A., Criado-Sudau, F.F., Gómez-Pujol, L., Tintoré, J., Orfila, A., 2023. Ten years of morphodynamic data at a micro-tidal urban beach: Cala Millor (Western Mediterranean Sea). Sci. Data 10. https://doi.org/10.1038/s41597-023-02210-2.

Gomes da Silva, P., Jara, M.S., Medina, R., Beck, A.L., Taji, M.A., 2024. On the use of satellite information to detect coastal change: demonstration case on the coast of Spain. Coast. Eng. 191. https://doi.org/10.1016/j.coastaleng.2024.104517.

Gómez-Pujol, L., Orfila, A., Álvarez-Ellacuría, A., Tintoré, J., 2011. Controls on sediment dynamics and medium-term morphological change in a barred microtidal beach (Cala Millor, Mallorca, Western Mediterranean). Geomorphology 132, 87–98. https://doi.org/10.1016/j.geomorph.2011.04.026.

González, M., Medina, R., Losada, M., 2010. On the design of beach nourishment projects using static equilibrium concepts: application to the Spanish coast. Coast. Eng. 57, 227–240. https://doi.org/10.1016/j.coastaleng.2009.10.009.

Hallermeier, R.J., 1977. Calculating a Yearly Limit Depth to the Active Beach Profile. Department of Defense, Department of the Army, Corps of Engineers, Coastal.

Hanson, H., Kraus, N.C., 1991. Numerical simulation of shoreline change at Lorain, Ohio. J. Waterw. Port, Coast. Ocean Eng. 117, 1–18.

Hanson, H., Larson, M., 1990. Numerical modeling of longshore and cross-shore sand transport. J. Coast Res. 407–429.

Harley, M.D., Andriolo, U., Armaroli, C., Ciavola, P., 2014. Shoreline rotation and response to nourishment of a gravel embayed beach using a low-cost video monitoring technique: San Michele-Sassi Neri, Central Italy. J. Coast Conserv. 18, 551–565. https://doi.org/10.1007/s11852-013-0292-x.

Harley, M.D., Turner, I.L., Short, A.D., 2015. New insights into embayed beach rotation: the importance of wave exposure and cross-shore processes. J Geophys Res Earth Surf 120, 1470–1484. https://doi.org/10.1002/2014JF003390.

Harley, M.D., Turner, I.L., Short, A.D., Bracs, M.A., Phillips, M.S., Simmons, J.A., Splinter, K.D., 2011a. Four decades of coastal monitoring at Narrabeen-Collaroy Beach: the past. Present and Future of This Unique Dataset.

Harley, M.D., Turner, I.L., Short, A.D., Ranasinghe, R., 2011b. A reevaluation of coastal embayment rotation: the dominance of cross-shore versus alongshore sediment transport processes, Collaroy-Narrabeen Beach, southeast Australia. J Geophys Res Earth Surf 116. https://doi.org/10.1029/2011JF001989.

Hart, D.E., Bryan, K.R., 2008. New Zealand coastal system boundaries, connections and management. N. Z. Geogr. 64, 129–143. https://doi.org/10.1111/j.1745-7939.2008.00133.x.

Jaramillo, C., González, M., Medina, R., Turki, I., 2021. An equilibrium-based shoreline rotation model. Coast. Eng. 163. https://doi.org/10.1016/j.coastaleng.2020.103789.

Jaramillo, C., Jara, M.S., González, M., Medina, R., 2020. A shoreline evolution model considering the temporal variability of the beach profile sediment volume (sediment gain/loss). Coast. Eng. 156. https://doi.org/10.1016/j.coastaleng.2019.103612.

Jiang, C., Zhang, S., Xie, Y., 2023. Constrained shuffled complex evolution algorithm and its application in the automatic calibration of Xinanjiang model. Front. Earth Sci. 10.

Klein, A., Benedet, L., Schumacher, D.H., 2002. Short-term beach rotation processes in distinct headland bay beach systems. J. Coast Res. 18, 442–458.

Lobato, F.S., Libotte, G.B., Platt, G.M., 2022. A novel multi-objective optimization method with local search scheme using shuffled complex evolution applied to mechanical engineering problems. Eng. Comput. 39, 2958–2989. https://doi.org/10.1108/EC-07-2021-0381.

McCarroll, R.J., Valiente, N.G., Wiggins, M., Scott, T., Masselink, G., 2023. Coastal survey data for Perranporth beach and Start bay in Southwest England (2006–2021). Sci. Data 10. https://doi.org/10.1038/s41597-023-02131-0.

Miller, J.K., Dean, R.G., 2004. A simple new shoreline change model. Coast. Eng. 51, 531–556. https://doi.org/10.1016/j.coastaleng.2004.05.006.

Montaño, J., Coco, G., Antolinez, J.A.A., Beuzen, T.O.M., Bryan, K., Cagigal, L., Castelle, B., Davidson, M., Goldstein, E., Vega, R.A.I.I., Idier, D., Ludka, B., Ansari, S. M., Mendez, F., Murray, B., Plant, N., Robinet, A., Rueda, A.N.A., Senechal, N., Simmons, J., Splinter, K., Stephens, S., Townend, I.A.N., Vitousek, S., Vos, K., 2019. Shorecasts: a blind-test of shoreline models. In: Coastal Sediments 2019. World Scientific, pp. 627–631. https://doi.org/10.1142/9789811204487_0055.

MOPT, 1991. Proyecto de Liquidacion de Obras de Emergencia de La Playa de Poniente de Benidorm (Alicante). General Service of Coasts of the State, Madrid.

Moriasi, D.N., Arnold, J.G., Van Liew, M.W., Bingner, R.L., Harmel, R.D., Veith, T.L., 2007. Model evaluation guidelines for systematic quantification of accuracy in watershed simulations. Trans. ASABE (Am. Soc. Agric. Biol. Eng.) 50, 885–900. https://doi.org/10.13031/2013.23153.

Morris, B.D., Turner, I.L., 2010. Morphodynamics of intermittently open–closed coastal lagoon entrances: new insights and a conceptual model. Mar. Geol. 271, 55–66. https://doi.org/10.1016/j.margeo.2010.01.009.

Nash, J.E., Sutcliffe, J.V., 1970. River flow forecasting through conceptual models part I — a discussion of principles. J. Hydrol. (Amst.) 10, 282–290. https://doi.org/10.1016/0022-1694(70)90255-6.

Neumann, B., Vafeidis, A.T., Zimmermann, J., Nicholls, R.J., 2015. Future coastal population growth and exposure to sea-level rise and coastal flooding - a global assessment. PLoS One 10. https://doi.org/10.1371/journal.pone.0118571.

Ojeda, E., Guillén, J., 2008. Shoreline dynamics and beach rotation of artificial embayed beaches. Mar. Geol. 253, 51–62. https://doi.org/10.1016/j.margeo.2008.03.010.

Palalane, J., Fredriksson, C., Marinho, B., Larson, M., Hanson, H., Coelho, C., 2016. Simulating cross-shore material exchange at decadal scale. Model application. Coast. Eng. 116, 26–41. https://doi.org/10.1016/j.coastaleng.2016.05.007.

Payra, S., Sharma, A., Verma, S., 2023. Chapter 14 - application of remote sensing to study forest fires. In: Kumar Singh, A., Tiwari, S. (Eds.), Atmospheric Remote Sensing. Elsevier, pp. 239–260. https://doi.org/10.1016/B978-0-323-99262-6.00015-8.

Pelnard-Considère, R., 1957. Essai de theorie de l'evolution des formes de rivage en plages de sable et de galets. Journées de l'hydraulique 4, 289–298.

Perez, J., Menendez, M., Losada, I.J., 2017. GOW2: a global wave hindcast for coastal applications. Coast. Eng. 124, 1–11. https://doi.org/10.1016/j.coastaleng.2017.03.005.

Rahnamay Naeini, M., Analui, B., Gupta, H., Duan, Q., Sorooshian, S., 2019. Three decades of the shuffled complex evolution (SCE-UA) optimization algorithm: review and applications. Sci. Iran. https://doi.org/10.24200/SCI.2019.21500.

Ratliff, K.M., Murray, A.B., 2014. Modes and emergent time scales of embayed beach dynamics. Geophys. Res. Lett. 41, 7270–7275. https://doi.org/10.1002/2014GL061680.

Reguero, B.G., Menéndez, M., Méndez, F.J., Mínguez, R., Losada, I.J., 2012. A Global Ocean Wave (GOW) calibrated reanalysis from 1948 onwards. Coast. Eng. 65, 38–55. https://doi.org/10.1016/j.coastaleng.2012.03.003.

Robinet, A., Idier, D., Castelle, B., Marieu, V., 2018. A reduced-complexity shoreline change model combining longshore and cross-shore processes: the LX-Shore model. Environ. Model. Software 109, 1–16. https://doi.org/10.1016/j.envsoft.2018.08.010.

Rodríguez-Santalla, I., Roca, M., Martínez-Clavel, B., Pablo, M., Moreno-Blasco, L., Blázquez, A.M., 2021. Coastal changes between the harbours of Castellón and Sagunto (Spain) from the mid-twentieth century to present. Reg Stud Mar Sci 46. https://doi.org/10.1016/j.rsma.2021.101905.

Short, A.D., 2006. Australian beach systems - nature and distribution. J. Coast Res. 22, 11–27. https://doi.org/10.2112/05A-0002.1.

Smith, R.K., Bryan, K.R., 2007. Monitoring beach face volume with a combination of intermittent profiling and video imagery. J. Coast Res. 23, 892–898. https://doi.org/10.2112/04-0287.1.

Splinter, K.D., Turner, I.L., Davidson, M.A., Barnard, P., Castelle, B., Oltman-Shay, J., 2014. A generalized equilibrium model for predicting daily to interannual shoreline response. J Geophys Res Earth Surf 119, 1936–1958. https://doi.org/10.1002/2014JF003106.

Thomas, T., Phillips, M.R., Williams, A.T., 2010. Mesoscale evolution of a headland bay: beach rotation processes. Geomorphology 123, 129–141. https://doi.org/10.1016/j.geomorph.2010.06.018.

Tintoré, J., Medina, R., Gómez-Pujol, L., Orfila, A., Vizoso, G., 2009. Integrated and interdisciplinary scientific approach to coastal management. Ocean Coast Manag. 52, 493–505. https://doi.org/10.1016/j.ocecoaman.2009.08.002.

Toledo, I., Pagán, J.I., López, I., Aragonés, L., 2022. Causes of the different behaviour against erosion: study case of the Benidorm Beaches (1956–2021). Mar. Georesour. Geotechnol. 41, 648–661. https://doi.org/10.1080/1064119X.2022.2084003.

Turki, I., Medina, R., Coco, G., Gonzalez, M., 2013a. An equilibrium model to predict shoreline rotation of pocket beaches. Mar. Geol. 346, 220–232. https://doi.org/10.1016/j.margeo.2013.08.002.

Turki, I., Medina, R., Gonzalez, M., Coco, G., 2013b. Natural variability of shoreline position: observations at three pocket beaches. Mar. Geol. https://doi.org/10.1016/j.margeo.2012.10.007.

Turner, I.L., Harley, M.D., Short, A.D., Simmons, J.A., Bracs, M.A., Phillips, M.S., Splinter, K.D., 2016. A multi-decade dataset of monthly beach profile surveys and inshore wave forcing at Narrabeen, Australia. Sci. Data 3, 160024. https://doi.org/10.1038/sdata.2016.24.

Vitousek, S., Barnard, P.L., Limber, P., Erikson, L., Cole, B., 2017. A model integrating longshore and cross-shore processes for predicting long-term shoreline response to climate change. J. Geophys. Res. Earth Surf 122, 782–806.

Wiggins, M., Scott, T., Masselink, G., Russell, P., McCarroll, R.J., 2019. Coastal embayment rotation: response to extreme events and climate control, using full embayment surveys. Geomorphology 327, 385–403. https://doi.org/10.1016/j.geomorph.2018.11.014.

Wright, L.D., Short, A.D., Green, M.O., 1985. Short-term changes in the morphodynamic states of beaches and surf zones: an empirical predictive model. Mar. Geol. 62, 339–364. https://doi.org/10.1016/0025-3227(85)90123-9.

Yates, M.L., Guza, R.T., O'Reilly, W.C., 2009. Equilibrium shoreline response: observations and modeling. J Geophys Res Oceans 114. https://doi.org/10.1029/2009JC005359.

Yu, Y., Megri, A.C., Miao, R., Hu, X., 2022. Calibrated dynamic zonal model DOMA+ using the SCE-UA method – application to atrium temperature distribution prediction. Sci Technol Built Environ 28, 1439–1455. https://doi.org/10.1080/23744731.2022.2118498.

Zhang, J., Larson, M., Ge, Z.P., 2020. Numerical model of beach profile evolution in the nearshore. J. Coast Res. 36, 506–520.